PROCESSING AND CHARACTERIZATION OF NANOCRYSTALLINE FeAl INTERMETALLIC COMPOUND PREPARED BY MECHANICAL ALLOYING

A Thesis Submitted

in Partial Fulfilment of the Requirements

for the Degree of

Master of Technology

by

NEERAJ MATHUR

to the

DEPARTMENT OF MATERIALS & METALLURGICAL ENGINEERING

INDIAN INSTITUTE OF TECHNOLOGY KANPUR

August, 1996

CERTIFICATE

It is certified that the work contained in the thesis entitled **"PROCESSING AND CHARACTERIZATION OF NANOCRYSTALLINE FeAl INTERMETALLIC COMPOUND PREPARED BY MECHANICAL ALLOYING"**, has been carried out under my supervision and that this work has not been submitted elsewhere for a degree.

Dr. Sanjeev Bhargava Dr. V.S.R. Murthy

DEPARTMENT OF MATERIALS & METALLURGICAL ENGINEERING

INDIAN INSTITUTE OF TECHNOLOGY KANPUR

25 MAY 1999 /MME

CENTRAL LIBRARY
I. I. T., KANPUR

Acc. No. A 128041

TH
MME/1996/m
M122f

A128041

ACKNOWLEDGEMENT

I express my deep sense of gratitude to Dr. Sanjeev Bhargava and Dr. V. S. R. Murthy for offering the opportunity to work with them and patiently guiding me throughout the course of this work.

Special thanks to my friends Sanjeev Shukla, Piyush Srivastava, Indira Kumar Dixit, Ashish Srivastava and Satyam Suwas, without their help and support this work would have not been possible.

I also thank Mr. B. Sharma, Mr. Uma Shankar Singh, Mr. G. S. Sharma, Mr. R. K. Prasad, Mr. Paul, Mr. R. P. Singh, Mr. K. P. Mukherjee and Dr. M. N. Mangole for being extremely helpful to me throughout my course of work.

There are also many with whom I have interacted during my stay at IIT Kanpur. All of them have contributed to my progress. I must acknowledge their support with utmost sincerity.

ABSTRACT

Elemental powders of iron and aluminium of purity > 99% and having average particle sizes of 100 μm and 50 μm respectively were used for synthesizing Fe-Al alloy powders, containing 47 at.% Al, corresponding to the B2 FeAl intermetallic compound by mechanical alloying route. The milling was performed in a high energy attritor mill with a ball to powder ratio of 10:1. The mill had a water cooling arrangement and toluene was used as the process - controlling agent. In order to follow the progress of mechanical alloying during milling, the milling of powders was carried out for different time intervals varying from 15 minutes to 235 hours. The powders thus produced were characterized using X-ray diffraction, optical and electron microscopy techniques. The XRD analysis of powders milled for different time intervals showed that instead of forming specific intermetallic compound(s), the product was found to be the solid solution of Fe-Al. Further analysis of the XRD data to reveal the crystalline size showed that the product had a nanocrystalline structure and that the contribution of strain increased as milling time increased. No amorphization of the product formed could, however, be obtained upto the milling time of 235 hours. Morphological analysis under optical and scanning electron microscopy showed that the mechanical alloying occurred by forming a lamellar structure. Also, powder morphology evolved from flaky shape in the initial stages of milling to a roughly equiaxed shape in the intermediate to final stages of milling. Mechanically alloyed powders were then consolidated using hot pressing technique. Densification of nearly 95% was observed by hot pressing the powders at a temperature of 1000°C and holding time of 20 min, under a constant applied pressure of 20 MPa. Some grain growth was observed in the hot pressed compacts but, however, the crystallite side remained in the nanometer range.

CONTENTS

List of Figures

CHAPTER - 1

INTRODUCTION

Ordered intermetallic compounds constitute a unique class of metallic materials that from long-range ordered crystal structures below a critical temperature that is generally referred to as the critical ordering temperature (Tc). These intermetallics usually exist in relatively narrow compositional ranges around simple stoichiometric ratios.

The search for new high temperature structural materials has stimulated much interest in ordered intermetallics. Recent interest has been focussed on aluminides of nickel, iron and titanium. These aluminides possess many attributes that make them attractive for high temperature structural applications. They contain enough aluminium to form in oxidising environments, thin films of aluminide oxides that often are compact and protective. They have low densities, relatively high melting points, and good high temperature strength properties.

Iron, nickel and titanium aluminides, like other ordered intermetallics, exhibit brittle fracture and low ductility at ambient temperatures. Poor fracture resistance and limited fabricability restrict the use of aluminides as engineering materials in most cases. Significant efforts have been devoted to understanding brittle fracture and poor ductility in these aluminides. As a result, both intrinsic and extrinsic factors that govern brittle fracture in the aluminides have been identified. Parallel alloy designs efforts have led to the development of aluminide alloys with improved mechanical and metallurgical properties at ambient and elevated temperatures.

The iron aluminides based on FeAl and Fe_3Al possess unique properties and have development potential as new materials for structural use. In addition to excellent corrosion resistance, the aluminides offer low material cost, low density, and conservation of strategic

elements. However, the major drawbacks of the aluminides are their low ductility and fracture toughness at ambient temperature and their poor strength at temperatures above 600°C. Recently, considerable efforts have been devoted to understanding and improving their mechanical properties through control of grain structure, alloy additions, and material processing.

Parallel to the above mentioned developments, in recent years novel material - processing methods have received much attention among scientists as one of the means of improving upon the properties of ordered intermetallic compounds. Non-equilibrium processing methods that result in metastable structures can often be used to synthesize materials with unique properties. One of these techniques is mechanical alloying (MA). This technique has been used to obtain supersaturated solid solutions, intermetallic phases, nanocrystalline alloys, amorphous alloy, high coercivity permanent magnets and quasicrystals from elemental crystalline powders mixtures. Nanocrystalline materials obtained by this technique can exhibit an excellent combination of properties making them potentially attractive for a number of applications.

CHAPTER - 2

LITERATURE REVIEW

2.1 ORDERED INTERMETALLIC COMPOUNDS

Ordered intermetallic compounds constitute a unique class of metallic materials that form long-range ordered crystal structures below a critical temperature, generally referred to as the critical ordering temperature (T_c). These ordered intermetallics usually exist in relatively narrow compositional ranges around simple stoichiometric ratios.

Ordered intermetallic alloys with relatively low critical ordering temperatures ($<700°C$) were studied quite extensively in the 1950s and 1960s, following the discovery of unusual dislocation structures and mechanical behavior associated with ordered lattices [1-3]. Deformation in ordered alloys is controlled by the glide of superlattice or paired dislocations, as illustrated in Fig. (2.1) for a two-dimensional ordered lattice having an AB composition. The first, or leading, dislocation creates a layer of antiphase domain (which can be thought of simply as a layer of wrong bonding), and the second, or following, dislocation restores the order. The relatively low mobility of superlattice dislocations at higher temperatures gives rise to anomalous yield behavior; that is, yield strength increases rather than decreases with increasing test temperature [4-11]. The anomalous yielding has been observed in many ordered intermetallics, such as Ni_3Al [4-6] and Cu_3Au [7] alloys. The results obtained by these studies are summarized in [2].

The interest in ordered intermetallics subsided in the latter part of the 1960s because of severe embrittlement problems encountered with the compounds. Most strongly ordered intermetallics are so brittle that they simply cannot be fabricated into useful structural

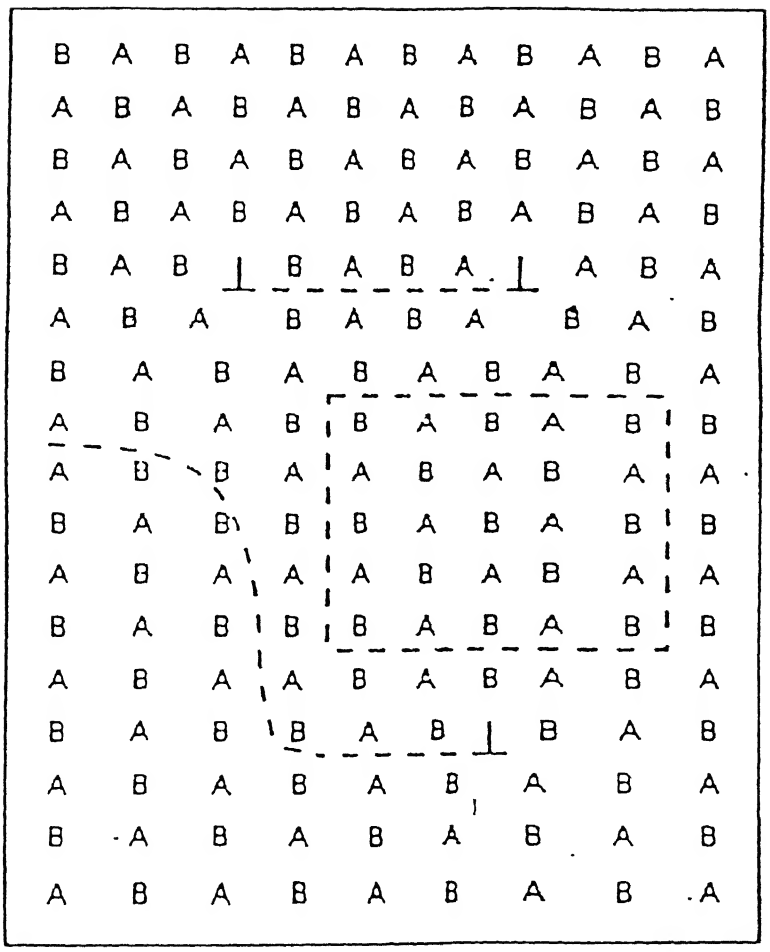

Fig. 2.1 Schematic Representation of a superlattice dislocation in a two-dimensional cubic lattice of ordered intermetallic compound of A and B

components [1-3,12]. Even when fabricated, these compounds have a low fracture toughness that severely limits their use as engineering materials. However, in the latter part of the 1970s, some prominent results were reported that showed that the ductility and fabricability of ordered intermetallics could be dramatically improved by alloy design efforts using physical metallurgy principles. The ductility of Co_3V was substantially improved by macroalloying with iron additions that reduced the average electron concentration and changed the ordered crystal structure from hexagonal to cubic [13-17]. The alloys $(Fe, Co, Ni)_3V$ with the cubic $L1_2$ ordered structure exhibited more than 40% ductility at room temperature [14]. The ductility of polycrystalline Ni_3Al was dramatically increased by microalloying with boron additions, which segregated to grain boundaries and suppressed brittle intergranular fracture [18,19]. Both cases have demonstrated the feasibility of achieving high tensile ductility in strongly ordered intermetallic alloys.

The recent search for new high-temperature structural materials has stimulated further interest in ordered intermetallics [20-22]. These compounds generally exhibit promising high-temperature properties because the long-range ordered superlattice lowers dislocation mobility and diffusion processes at elevated temperatures [1-3,20-22]. However, because of the brittleness problem, the intermetallics have been used mainly as strengthening constituents in structural materials. For example, high temperature nickel base superalloys owe their outstanding strength properties to a fine dispersion of precipitated particles of the ordered γ' phase (Ni_3Al) embedded in a ductile disordered matrix.

Recent research has focused on understanding the brittle fracture and low ductility in ordered intermetallics [1-3,20-27]. Possible causes for brittleness include:

* Insufficient number of deformation modes
* High yield strength or hardness caused by difficulty in the generation and glide of dislocations
* Poor cleavage strength or low surface energy
* Planar slip and localized deformation
* High strain rate sensitivity (which promotes brittle crack propagation at crack tips)
* Grain boundary weakness
* Environmental embrittlement

In some cases, the brittleness results from strong resistance to the motion of dislocations, to the point that cleavage or intergranular fracture may be favored. In many cases, however, the dislocations are relatively mobile. Brittleness results either from low-symmetry crystal structures that do not possess enough independent slip systems to permit arbitrary deformation or from the presence of grain boundaries that are too weak to resist the propagation of cracks. Recently, it has been found that quite a number of ordered intermetallics, such as iron aluminides [26,27], exhibit environmental embrittlement at ambient temperatures. The embrittlement involves the reaction of water vapor in air with reactive elements (aluminium, for example) in intermetallics to form atomic hydrogen, which drives into the metal and causes premature fracture.

In recent years, alloying and processing have been employed to control the ordered crystal structure, microstructural features, and grain-boundary structure and composition to overcome the brittleness problem of ordered intermetallics [20-22]. Success in this work has inspired parallel efforts aimed at improving mechanical properties. The results have led to the development of a number of attractive intermetallic alloys having useful ductility and strength.

Alloy design work has been centred primarily on aluminides of nickel, iron, and titanium [20-22]. These materials possess a number of attributes that make them attractive for high-temperature applications. They contain sufficient amounts of aluminum to form, in oxidizing environments, thin films of alumina (Al_2O_3) that often are compact and protective [28], These materials have low densities, relatively high melting points, (Table 2.1) and good high temperature strength properties.

Crystal structures showing the ordered arrangements of atoms in several of these aluminides are illustrated in Fig. (2.2). Deviations from stoichiometry are accommodated either by the incorporation of vacancies in the lattice (for example, NiAl) [29-32] or by the location of antisite atoms in one of the sublattices. Many of the aluminides exist over a range of compositions, but the degree of order decreases as the deviation from stoichiometry increases. Additional elements can also be incorporated without losing the ordered structure. For example, in Ni_3Al, silicon atoms are located on aluminum sites, cobalt atoms on nickel sites, and iron atoms on either [33]. In many instances, the so-called intermetallic compounds can be used as bases for alloy development to improve or optimize properties for specific applications.

Many of the aluminides suffer from low-temperature (room temperature) embrittlement, which has been severe enough to preclude their use as structural materials. In several cases, however, metallurgical solutions have been discovered that offer the possibility of engineering applications [20-22].

2.2 IRON ALUMINIDES

Iron aluminides have been of interest since the 1930s when their excellent corrosion resistance was first noted [34]. Since the observation of Bradley and Jay, research has continued on these materials to improve their room temperature ductility and strength above 600°C. All

Table 2.1

Properties of Nickel, Iron and Titanium Aluminides

Alloy	Crystal Structure(s)	Critical Ordering Temperature (T_c)	Melting Point (T_m)	Material density
		°C	°C	g/cm^3
Ni_3Al	$L1_2$ (ordered fcc)	1390	1390	7.50
NiAl	B2 (ordered bcc)	1640	1640	5.86
Fe_3Al	DO_3 (ordered bcc)	540	1540	6.72
	B2 (ordered bcc)	760	1540	-
FeAl	B2 (ordered bcc)	1250	1600	5.56
Ti_3Al	DO_{19} (ordered hcp)	1100	1600	4.2
TiAl	$L1_o$ (ordered tetragonal)	1460	1460	3.91

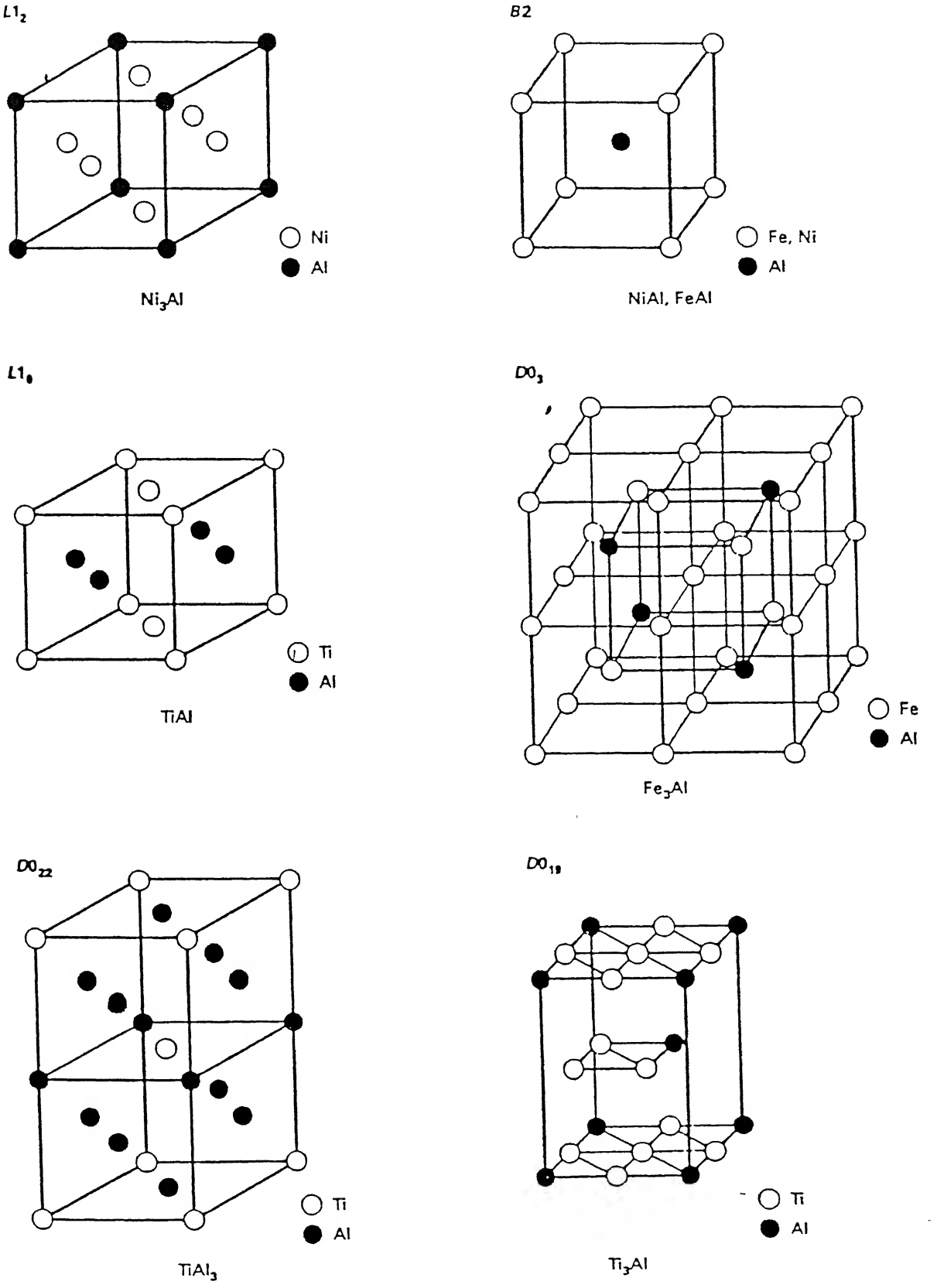

Fig. 2.2 Crystal Structures of nickel, iron and titanium aluminides

of these have resulted in significant contributions to the fabrication and mechanical properties of iron aluminides.

2.2.1 Phase and Crystal Structure

The Fe-Al system is characterized by a wide α-Fe solid solution range upto about 18 at% Al at room temperature. With increasing aluminium, however, various stable phases occur namely, Fe_3Al, FeAl, $FeAl_2$, Fe_2Al_5 and $FeAl_3$. Each of these has a homogeneity range as shown in Fig. (2.3). Iron aluminide form bcc ordered crystal structures over the composition range of 25 to 50 at% Al [35]. From the phase diagram it is evident that Fe_3Al exists as ordered DO_3 structure upto 540°C and as ordered B2 structure between 540°C and 760°C, the structure of the phase is disordered bcc.

There are two ordered phases of interest, Fe_3Al and FeAl, which have DO_3 and B2 ordered superlattice structures respectively. Both of these ordered structure are shown in Fig. (2.2), [36,37]. The DO_3 structure consists of eight bcc cells in which out of 16 atoms of the unit cell, 4 atoms are of aluminium atoms, at (3/4, 3/4, 3/4), (3/4, 1/4, 1/4), (1/4, 3/4, 1/4), (1/4, 1/4, 3/4) lattice sites; remaining sites being occupied by 12 iron atoms. Although, disordered structure is bcc, the ordered structure has symmetry as of fcc structure owing to tetrahedral arrangement of aluminium in the unit cell. B2 structure on the other hand has two interpenetrating simple cubic lattice with the atoms of each constituent at the body center of the other. Thus, iron atoms at (0,0,0) and aluminium at (1/2, 1/2, 1/2) lattice sites. The DO_3 (Fe_3Al) order exist over the range of 18 at% to nearly 36 at%, whereas the B2 (FeAl) order occurs from 36 at% to 50 at% aluminium composition range.

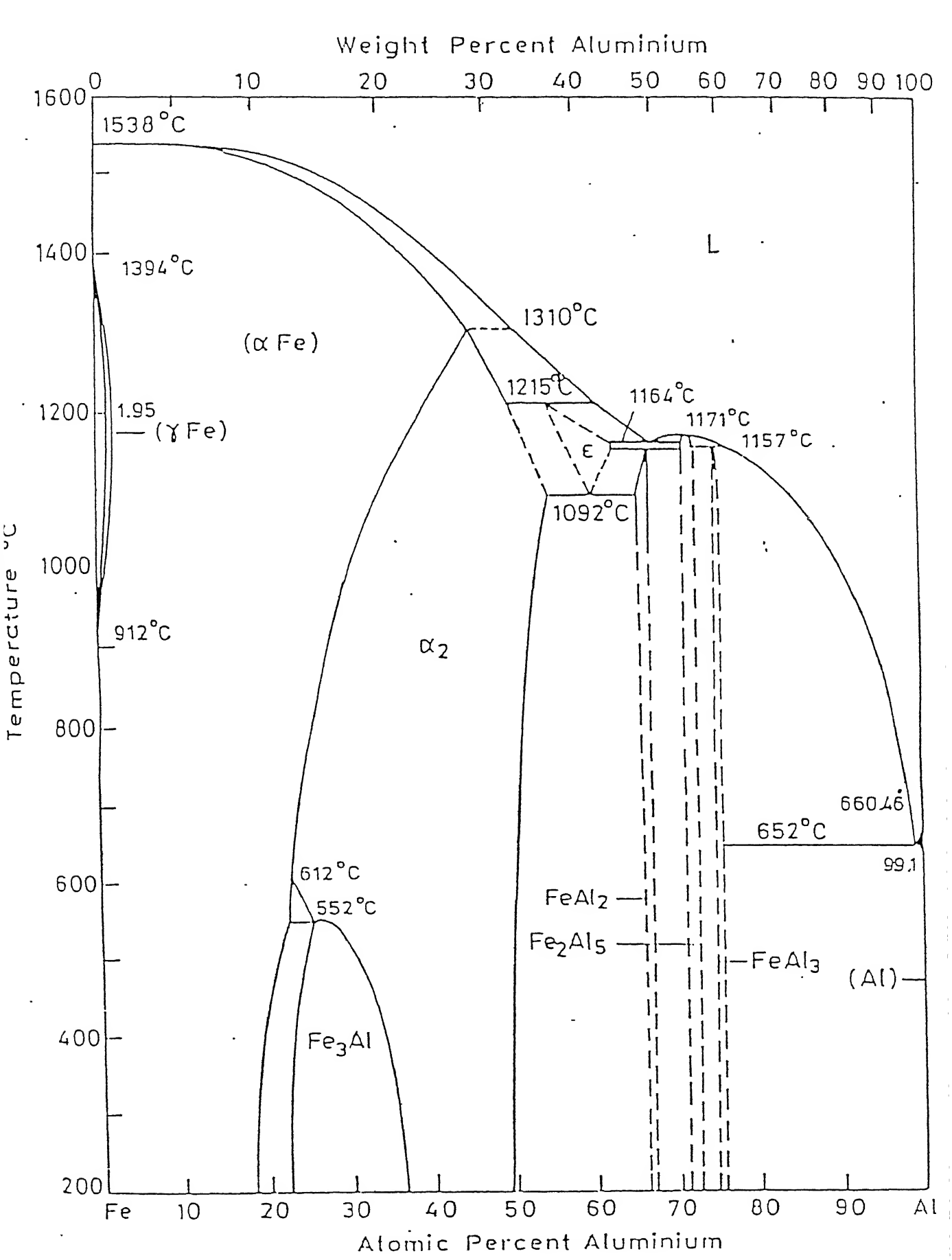

Fig. 2.3 Iron-Aluminium Phase Diagram

2.2.2 Mechanical Behavior of FeAl and Fe_3Al

The aluminides show low ductility and brittle fracture at room temperature and their fracture mode depends on aluminium concentration. The aluminides containing less than 40 at% Al exhibit mainly transgranular cleavage fracture, whereas those with more than 40% Al show essentially brittle intergranular fracture [38-40]. The fracture mode is also sensitive to other parameters such as grain size and impurities. Fe_3Al (25 at% Al) has been reported to fracture intergranularly when it contains excess carbon [41]. Also, some FeAl alloys with less than 40% Al show grain boundary fracture when prepared by P/M techniques and contaminated with oxygen [42].

Mechanical properties of the iron aluminides have been characterized as functions of test temperature and alloy composition in a number of studies [38-42]. In general, yield strength is not sensitive to temperature below 600 to 650°C; above that temperature range, strength shows a sharp drop with temperature. For intermediate and coarse-grain materials, the aluminides with less than about 40% Al generally show a small increase in yield strength with temperature, with strength reaching a peak at temperatures of about 550 to 650°C. For the aluminides with higher levels of aluminium, the increase in yield strength is suppressed, possibly because of grain - boundary sliding at elevated temperatures [38,40,42].

2.2.3 Ductility and Slip Behavior

In terms of ductility, the aluminides with less than 40% Al have a room - temperature tensile elongation of about 2 to 4% for coarse - grain materials (that is, materials with grain sizes of 150 to 200 μm) [26]. Elongation increases to 6 to 8% when the grain structure is refined [43], indicating the effect of grain size on the ductility. A recent study found that the

ductility of FeAl with 40% Al was substantially improved by mechanical alloying [44]; the mechanical alloying probably reduced the grain size, thereby reducing the tendency toward brittle intergranular fracture. The ductility of aluminides with up to 30% Al increases with test temperature and reaches more than 40% at 600°C. Aluminides with more than 35% Al show a decrease in ductility above 600°C and reach a minimum ductility around 750°C. The decrease in ductility is believed to be caused by cavitation in the grain-boundary region when the aluminides are tested under tension [38,42].

The aluminides, like iron and steels, slip by {111} dislocations at ambient temperatures. However, the slip changes to {100} type at elevated temperatures. The transition depends on the aluminium concentration [45,46], with a general trend of decreasing transition temperature with increasing aluminium level. For example, a transition temperature of about 1000°C was reported for the 35% Al alloy; the transition temperature was below 400°C for the 50% Al alloy [45]. There is no sharp change in ductility around the transition temperature.

2.2.4 Environmental Embrittlement

Iron aluminides have been known to be brittle at room temperature for more than 50 years; however, the major cause of their low ductility and brittle fracture was not identified until recently. The study of the environmental effect on tensile properties indicates that the poor ductility commonly observed in air tests is caused mainly by an extrinsic effect - environmental embrittlement. The yield strength is insensitive to environment, and the ultimate tensile strength correlates with the tensile elongation, which depends strongly on test environment. The aluminide had ductilities of 2% in air, 6% in vacuum, and 17.6%in dry oxygen. The water-vapor test confirmed the low ductility found in the air tests, indicating that moisture in air is the embrittling agent. The increase in ductility from 2% to 18% is accompanied by a change in

fracture mode from transgranular cleavage in air to mainly grain boundary separation in dry oxygen. This suggests that cleavage planes in FeAl are more susceptible to embrittlement than are the grain boundaries.

Environmental embrittlement has been explained by the following chemical reaction:

$$2Al + 3H_2O \rightarrow Al_2O_3 + 6H \quad (1)$$

The reaction of moisture in air with aluminium atoms at crack tips results in the generation of high-fugacity atomic hydrogen that rapidly penetrates into the crack tips and causes severe embrittlement. The fact that the yield strength is insensitive to ductility and test environment is consistent with the mechanisms of hydrogen embrittlement that were observed in other ordered intermetallic alloys [47-55].

2.2.5 Alloying Effect in FeAl Aluminides

FeAl aluminides containing 40% or more aluminum fail at room temperature by integranular fracture with little tensile ductility [38,42]. Small additions of boron (0.05 to 0.2%) suppress grain boundary fracture and allow a small increase in ductility (~3%) of Fe-40Al, but not of Fe-50Al [56]. The beneficial effect of boron is not nearly as dramatic in FeAl as it is in Ni_3Al, but it is nevertheless significant. The ductility of boron-doped FeAl aluminides remains low because the alloys are still embrittled by the test environment (air). It has been found recently that boron-doped FeAl (40% Al) exhibits a high ductility (18%) when tested in dry oxygen to avoid environmental embrittlement.

Boron additions also increase the elevated - temperature strength of FeAl, especially in combination with niobium and zirconium. For example, the creep rate can be lowered by an order of magnitude at 825°C by the combination of 0.1%Zr and 0.2% B [57]. Measurements

of the activation energy for creep indicate that additions act by slowing diffusional processes rather than through precipitation reactions. Partial replacement of iron with nickel improves the creep properties of FeAl at high temperatures [58].

2.2.6 Weldability and Corrosion Resistance

Other properties of iron aluminides, including weldability [78] and corrosion resistance, have been characterized to a limited extent. Fe_3Al is weldable with careful control of welding parameters and minor alloy additions. Additions of TiB_2 promote hot cracking and are detrimental to the weldability of Fe_3Al aluminides. Sound weldments have been achieved in Fe_3Al alloys using both electron beam and gas tungsten arc welding processes.

The iron aluminides are highly resistant to oxidation and sulfidation at elevated temperatures [60,61]. This resistance stems from the ability of the aluminides to form highly protective Al_2O_3 scales. The oxidation resistance generally increases with increasing aluminum content; the major products are α -Al_2O_3 and trace amounts of iron oxides when the aluminides are oxidized at temperatures above 900°C [60]. Cyclic oxidation of Fe-40Al alloyed with up to 1 at% Hf, Zr, and B produced little degradation at temperatures up to 1000°C. Aluminide specimens tested at 700 and 870°C showed no indication of attack in sulfidizing environments, except for the formation of a thin layer of oxides with a thickness in an interference color range. The iron aluminide alloys exhibited corrosion rates lower than those of the best existing iron-base alloys (including coating material) by a couple of orders of magnitude when tested in a severe sulphidizing environment at 800°C.

2.2.7 Multiphase Materials Based on Iron Aluminides

2.2.7.1 Iron Aluminide Plus Coherent Particles

DO_3 Fe-Al alloys may be age hardened as a result of bcc/DO_3/B_2 phases co-existing coherently [62] (Fig. 2.7). The peak yield strength depends on the composition and temperature and has a value of approximately 400 MPa at 833 K for Fe-24 Al and 873 K for Fe-26% Al. Ti substitution for Fe increases the B2 and DO_3 ordering temperature and also expands the α + DO_3 phase field [63]. Significant precipitation strengthening at elevated temperatures has been reported to result from Ti additions (Fe-25%Al-5%Ti Alloy), though the room temperature ductility was sharply reduced.

Precipitation hardening in DO_3 Fe-25%Al-2%Nb may be achieved through formation of a coherent metastable $L2_1$ phase. Significant (upto 50%) strengthening compared with as-extruded Fe_3Al temperature up to 873 K was reported. Additions of 2% Ti increased from 16 to 1000 h the time for which coherent precipitates were retained at 1023K.

2.2.7.2 Reinforced Iron-Aluminides

Heat treatments at 1000 to 1500 K for up to 1000 h carried out on Fe-40%Al-ceramic fibre (SiC, B_4C, W, Mo-based and Al_2O_3) composites revealed that thermodynamic calculations [64] were successful in predicting chemical compatibility [65]. However, the predicted reaction mode was not always observed due to the formation of ternary reaction products. W and Al_2O_3 fibres were found to be the least reactive with Fe-40Al but porosity in W fibres arising from the Kirkendall effect limited its usefulness. Moser et al. [66] have classified ceramics into three categories after HIPping and heat treating FeAl-ceramic particulate mixtures at 1498 K. 'Highly-

reactive systems': i.e. those which form reaction products (e.g. FeAl/B_4C) or 'Non-reactive systems': i.e., those with weak bonding FeAl and ceramic (e.g. FeAl/Al_2O_3) were classed as unsuitable. The ideal systems were 'partially reactive' where there is some compositional or structural change to provide bonding but no large scale, third phase, reaction products. FeAl/TiB_2 system was considered promising because of good bonding between FeAl and TiB_2 arising from diffusion of Fe into TiB_2 particles.

Despite these compatibility studies, literature on properties of such reinforced alloy is limited. Vedula and co-workers [67-69] have dispersion strengthened Fe-40%Al by milling prealloyed Fe-40%Al-0.1%Zr Powder with B and Y_2O_3 powders. Incomplete mixing was observed. Hot extrusion resulted in homogeneous structure with a fine Y_2O_3 dispersion. The extruded grain sizes (3 to 6 μm) were finer than those (8 to 15 μm) observed in alloys without dispersoids. It was proposed that dispersoids encourage nucleation of new grains during recrystallisation. The fine grain size was shown to be beneficial to properties both at room temperature and high temperature.

2.3 MECHANICAL ALLOYING

Mechanical alloying is a solid state powder processing technique which involves milling of pure metal mixures in high energy ball mills. During high energy ball milling, repeated welding, fracturing and rewelding of powder particles takes place which results in the formation of highly deformed particles containing alternate layers of different constituents of the original elemental blend. These fine-layered structures aided by deformation induced defects enhance the diffusion rates and thus result in alloying. This technique was originally developed, by Benjamin and coworkers [70], to produce oxide dispersion strengthened (ODS) Ni and Fe base

superalloys and Al alloys which were found to be much superior in their high temperature strength when compared to cast and wrought superalloys and SAP alloys respectively. It has been shown by several investigators that MA can be effectively used to synthesize all the metastable structures that are possible by rapid solidification processing (RSP), viz. extension of terminal solid solubility, metastable crystalline, quasicrystalline and amorphous phases. In addition mechanical alloying has resulted in the synthesis of nanocrystalline structures and extension of solid solubility in the liquid immiscible systems which are difficult to be achieved by RSP.

2.3.1 Types of Mills used for Mechanical Alloying

The mills used for Mechanical alloying are usually of three types [71]. One is a vertical ball mill such as the Szegvari attritor (Fig. 2.4(a)), which can be used to produce moderate volumes of material in "moderate" milling times (typically, on the order of hours). In this device, the ball and powder charges are held in a stationary vertical tank and are agitated by impellers radiating from a central rotating shaft.

A second configuration is the vibratory mill, exemplified by the SPEX shaker mill (Fig. 2.4(b)). Such a machine can produce small quantities of mechanically alloyed powder in relatively short times (typically, in less than an hour). In this system, the ball and powder charges are placed in a small vial which is agitated at a high frequency in a complex cycle which involves motion in three orthogonal directions.

A third type of machine that can be used for mechanical alloying is a conventional horizontal ball mill (Fig. 2.4(c)). In such a mill, the powder and ball (long rods are sometimes used) charges are placed in a large (>1 m in diameter) drum, which is rotated about its central horizontal axis at a speed just below the critical speed that would pin the balls to the internal

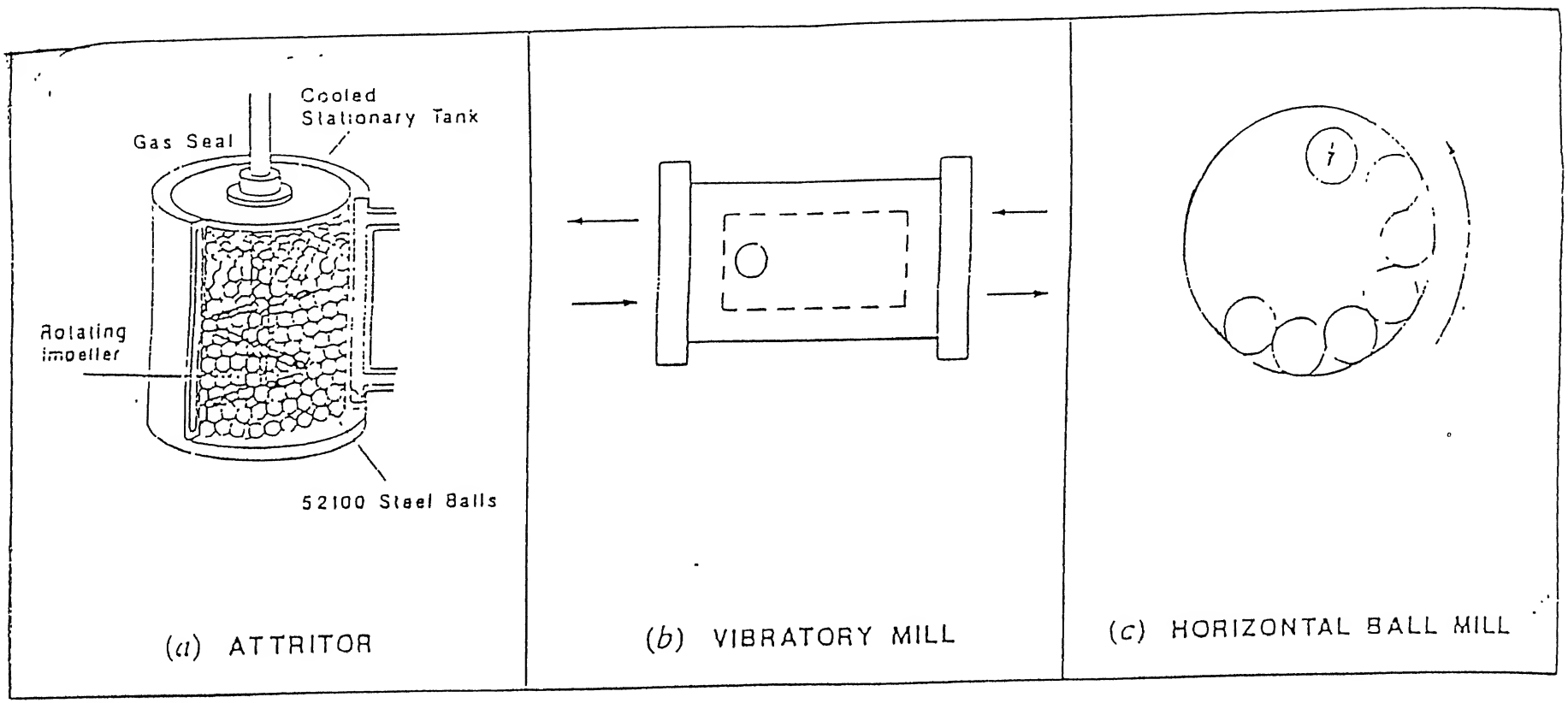

Fig. 2.4 Types of Mills used for Mechanical alloying (a) An attritor (b) SPEX Shaker (or vibratory mill) (c) a conventional ball mill

wall of the drum. Mills of this nature are used to produce large volumes of powder, but the processing times are typically long (on the order of days or more).

Regardless of the mill used, the mechanical alloying process is characterized by collisions between tool and powder which result in powder fragmentation and coalescence. There are several possible geometries for such collisions. For example, powder may be trapped between two colliding balls or caught between a ball and the wall of the container. And in the case of the vertical ball mill, powder may be impacted between the grinding media balls and the rotating impellers.

The attritor (i.e., the vertical mill) has probably been the most widely used device for laboratory investigations. On geometrical considerations, it is clear that the greatest number of collision events in this system are of the ball - powder - ball type. This kind of impact has been the basis for qualitative descriptions of the mechanical alloying process.

2.3.2 Mechanism of Mechanical Alloying

The Mechanical Alloying process is described as consisting of several stages, as schematized in Fig. (2.5) [72]. (It must be understood that mechanical alloying is statistical in nature, however; thus, each particle experiences a unique processing history). The first stage involves powder mixing and concurrent deformation, fracture, and welding of powder particles. The deformation and welding cause the formation of large flake shaped particles and composite particles containing layers of the alloy components. A significant variability is seen in the morphology and hardness of the particles during this stage due to the statistical nature of the process.

In the next stage, the welding of powder particles dominates. Thus, the particle size increases and the number of particles decreases concurrently. Particle hardness continues to

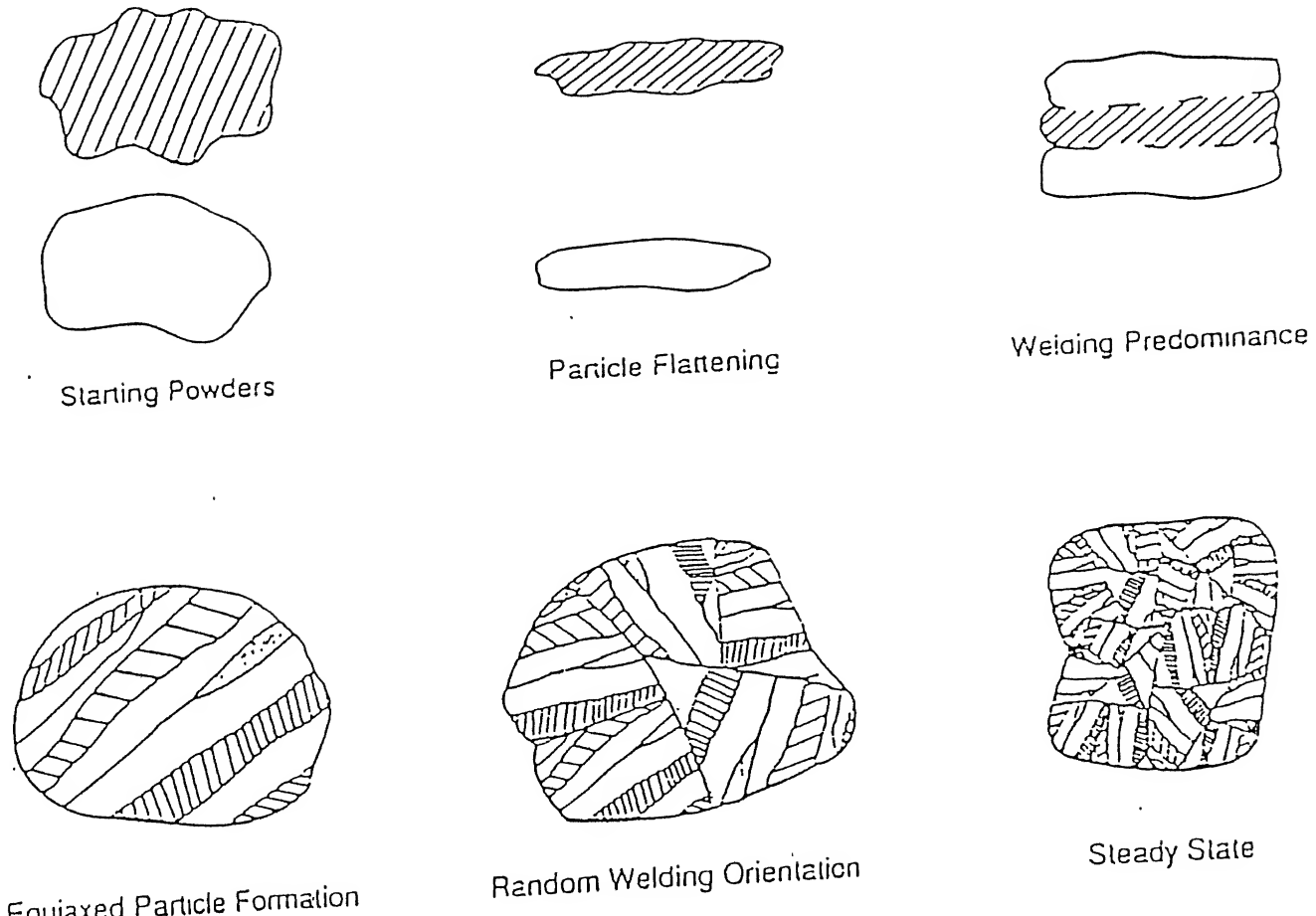

Fig. 2.5 Schematic of stages of Mechanical alloying

increase due to the extensive plastic deformation taking place during mechanical alloying. The subsequent two stages are those of equiaxed particle formation and welding of layered particles producing "random" particle orientations. During these stages, there is a decrease in the fraction of large flake - shaped particles and the lamellar structure of the particles not only becomes progressively finer but also manifests a convoluted or marbled (Damascus steel) structure. The continuing increase in particle hardness and concurrent decrease in ductility lead to an increased tendency for particle fracture.

Steady-state processing constitutes the final mechanical alloying stage. The composition of each particle converges to the over all composition, and hardness approaches a saturation value, as seen in Stage IV of work hardening. During steady - state processing, there is a reasonable balance between the frequencies of particle fracturing and welding. Thus, the average particle size does not change much during this stage nor does the distribution in particle sizes.

2.3.3 Formation of Nanocrystalline Structures by Mechanical Alloying

Metallurgists and materials scientists have been conducting research investigations for several centuries to develop materials which are 'stronger, stiffer, and lighter' than the existing materials and also capable of use at elevated ('hotter') temperatures. Several novel and non-equilibrium processing methods have been developed during the past few decades to improve the performance of the existing materials; these include mechanical alloying [73], rapid solidification from the liquid state [74,75], plasma processing [76], vapour deposition [77], etc. A central underlying theme in all these methods is to energize the material to bring it into a highly non-equilibrium (metastable) state (also including a possible change of state from the solid to liquid or gas) through melting, evaporation, irradiation, application of pressure, storing of mechanical

energy, etc. [78]. The materials is then brought to another lower-energy metastable state by quenching or related processes when it can exist as a supersaturated solid solution, metastable crystalline or quasicrystalline phase, or even in a glassy state, affording ample opportunities to modify the crystal structures and/or microstructrures. These processes have led to considerable improvement in the properties of a number of alloy systems and consequently some industrial applications; these have been described and fully documented in the references listed above.

A novel way of transforming a material to a metastable state is to reduce its grain size to very small values of a few nanometers (1 nm = 10^{-9}m) when the proportion of atoms in the grain boundaries is equivalent to or higher than those inside the grains. Materials with such small grain sizes are now referred to as nanocrystalline materials (and also as nanocrystals, nanostructures, nanophase materials, or nanometer-sized crystalline solids), and have been shown to have properties vastly superior to those exhibited by conventional grain - sized (> 10 μm) polycrystalline materials. It is the combination of unique compositions and novel microstructcures that leads to the extraordinary potential of the nanocrystalline materials.

There has been a continued increase in the research investigations in recent years on the synthesis/processing, characterization, properties, and potential applications of these novel materials.

Nanocrystalline materials are single-phase or multi-phase polycrystals, the crystal size of which is of the order of a few (typically 1 to 100) nanometers in at least one dimension. Thus, they can be basically equiaxed in nature and will be termed nanostructure crystallites (three dimensional [3-d] nanostructures), or they can consist of a lamellar structure, and will be termed a layered nanostructure (one-dimensional [1-D] nanostructure), or they can be filamentary

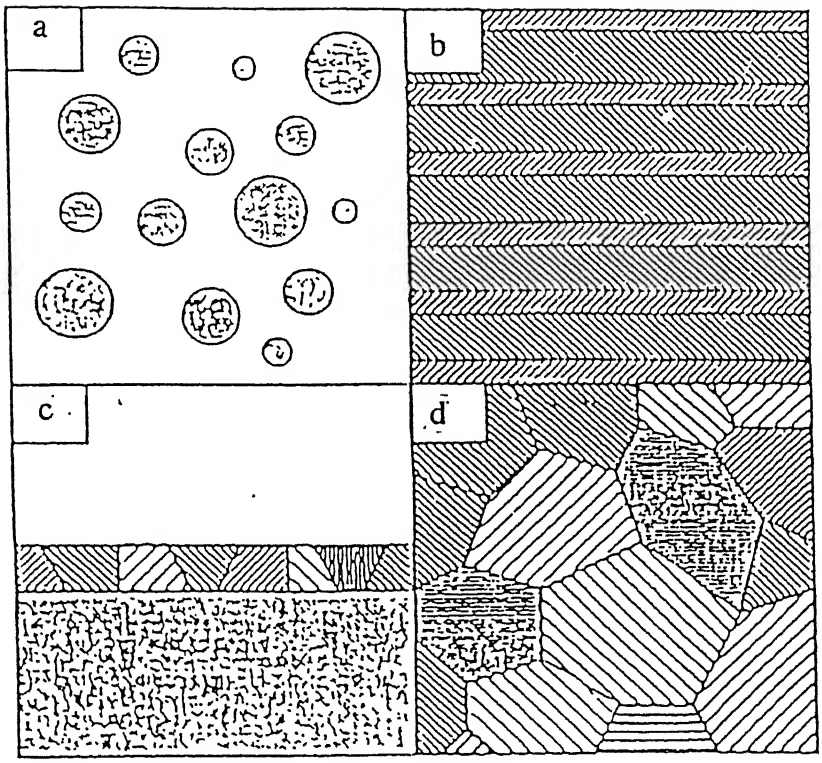

Fig. 2.6 Schematic of the four types of nanocrystalline materials : (a) clusters (b) layered (lamellar) (c) filamentry and (d) crystallites (equiaxed)

in nature (two-dimensional [2-D] nanostructure). Additionally Siegel considers zero-dimensional atom clusters and cluster assemblies. Fig. 2.6 illustrates the four types of nanostructures schematically. The magnitudes of length and width are much greater than thickness in the layered nanocrystals, and length is substantially larger than width or diameter in filamentary nanocrystals. The nanocrystalline materials may contain crystalline, quasicrystalline, or amorphous phases and can be metals, ceramics, or composites.

Amongst the above, maximum attention has been paid to the synthesis, consolidation, and characterization of the 3D-nanostructured crystallites followed by the 1D-layered nanostructures. While the former are expected to find applications based on their high strength, improved formability, and a good combination of soft magnetic properties, the latter are visualized for electronic applications. Relatively few investigations have been carried out on the 2D-filamentary nanostructures and it is only recently that zero-dimensional clusters are being investigated to tailor the optical properties.

Increased activity on the synthesis of nanocrystalline materials in recent years dates back to the pioneering investigations of Herbert Gleiter of the University of Saarlandes in Germany in 1981. He synthesized ultrafine nanometer-sized metallic particles using an inert gas condensation technique and consolidated them in situ into small disks under ultra-high vacuum conditions. Since then a number of techniques have been developed in which the starting material can be either in the solid, liquid, or gaseous states.

In principle, any method capable of producing very fine grain-sized polycrystalline materials (by increasing the nucleation rate and reducing the growth rate during formation) can be utilized to produce nanocrystalline materials. The methods which have been commonly employed to synthesize these materials include inert gas condensation [79], spray conversion

processing [80], sputtering [81], electrodeposition [82], co-precipitation [83], sol-gel process [84], sliding wear [85], spark erosion [86], plasma processing [87], laser ablation [88], hydrothermal pyrolysis [89], and thermophoretic forced flux system [90]. The grain size, morphology, and texture can be varied by suitably modifying/controlling the process variables in each of these methods.

Widespread application of nanocrystalline materials requires production of the powder in tonnage quantities and also efficient methods of consolidating the powders into bulk shapes. Mechanical alloying, is a proven commercial process to produce oxide-dispersion-strengthened nickel- and iron-base superalloy powders [91] and can be easily adapted to produce nanocrystalline powders on a commercial scale.

Recent studies have shown that nanocrystalline materials can be synthesized by high energy ball milling of elemental powders [92-94], intermetallic compound powders [92,95,96], or powders of immixible alloy systems [93,97-99]. Fecht et al [93] developed nanocrystalline structures in various elemental b.c.c. and h.c.p. metal powders by ball milling. Schlump et al [97] have reported on the formation of nanocrystalline structures in metal-metal systems and metal-metalloid system. In metal-metal systems they have reported that powders with nanocrystalline structures can be formed only in the composition range lying outside of the region in which metastable solid solutions form (determined by milling). This applied to ODS-alloys on the basis of Ni and Al and even to systems like Fe-Ta, as for as these were investigated. In Fe-Ta system, they observed, that addition of 5 wt% W (tungsten) resulted in a crystalline structure with grain size of less than 10 nm. In Ti-Ni system, a mixture of nanocrystalline α-Ti and Ni crystals embedded in an amorphous matrix formed when the composition was selected in the metastable two-phase region amorphous - crystalline. Even

cermets (Ceramic-metal compounds) having nanocrystalline structures, have been produced by mechanical alloying. Cermets powders with nanocrystalline structures were obtained in Ti-Ni-C, V-Ni-C and Si-Ni-C systems by Schlump et al. Shingu et al [100] obtained nanocrystalline structures for Al-24.4 wt% Fe and Ag 56.3 wt% Fe alloys by Mechanical alloying of elemental powder mixtures.

2.3.4 Amorphization by Mechanical Alloying

The fundamental research using mechanical alloying during the last several years has been dominated by the use of this technique for solid state amorphization. It is convenient to divide amorphization by ball milling into the categories of 1) mechanical alloying (MA) of elemental (or dissimilar alloy) powders involving material transfer between the components, and 2) mechanical milling (MM) of a single composition (e.g. an intermetallic compound, an immiscible mixture, or an element) such that no material transfer need occur. Some investigators prefer to use "mechanical grinding" (MG) for the latter process.

The first examples of amorphization of intermetallic compounds by mechanical milling were presented by Ermakov et al. [101,102] in the Y-Co and Gd-Co systems. Intermetallics such as YCo_3, Y_2Co_7, YCo_5 and Y_2Co_{17} where milled and found to exhibit the broad diffraction peak and Mossbauer spectra of an amorphous alloy. Milling of $GdCo_3$ and Gd_2Co_7 resulted in a two phase (amorphous + crystalline) structure. Subsequently a number of intermetallic compounds have been amorphized by milling and are reported in the review of Weeber and Bakker [103].

The first suggestion that mechanical alloying might produce amorphous material was made by White [104] during a study of the synthesis of superconducting Nb_3Sn via MA and subsequent thermomechanical treatment. The first definitive study of amorphization by MA was

carried out by Koch et al [105] in the easy-glass-forming alloy system Ni-Nb. Since then, a number of alloys have been amorphized by MA, and the details for the various systems are given int he review of Weeber and Bakker up to 1988. A recently investigated system in which MA has induced amorphization is 80 Al + 20 Fe (Wang et al, [106]). Although the detailed mechanisms for amorphization by either MM or MA are not yet well defined, working hypotheses have been developed from which to predict experimental results.

In trying to understand the amorphization mechanism during MA, earlier investigators assumed that the rate of plastic deformation of the powder particles trapped between milling balls was so high that parts of the particles melted. Following the collisions, these melt pools would solidify rapidly by heat conduction into the less deformed, and thus cooler, interior regions of the particles. Thus, the amorphous alloy would form by a cumulative rapid solidification process. It was soon after realized [107-109] that the local temperature increase was at most a few hundred Kelvin. Researchers now believe the amorphization during MA is not a purely a mechanical process and that a solid state amorphization reaction (SSAR) similar to that observed in this films occurs during mechanical alloying. It is in general accepted that two criteria should be fulfilled by any binary system for SSA (Schwarz and Johnson) [110]. First, the heat of mixing in the amorphous phase, which is assumed to be the supercooled liquid for most of the thermodynamic calculations, should be more negative when compared to that of crystalline solid solution thus providing a chemical driving force for its formation. Secondly, the diffusivity of one element in the other should be anamolously fast so that nucleation and growth of more stable intermetallic compounds is kinetically constrained.

Schwarz et al [111] observed amorphization by mechanical alloying of Ni and Ti powders at an average composition of $Ni_{33}Ti_{67}$. Dolgin et al 112] observed growth of amorphous

phase during mechanical alloying of $Ni_{50}Ti_{50}$, $Co_{50}Ti_{50}$ and $Fe_{50}Ti_{50}$. Similarly many of the same alloy systems which undergo SSAR are also found to amorphize by mechanical alloying.

It has also been found that there are several alloys which can be amorphized by mechanical alloying but not by SSAR of thin film diffusion couples. These included $Nb_{50}Al_{50}$ [113] and $Nb_{75}Ge_{25}$ [114]. In the case of $Nb_{75}Ge_{25}$ the mechanism for amorphization can be classified with amorphization of intermetallic compounds by mechanical milling, since for Nb and Ge powders mechanical alloying first forms the A15 structure Nb_3Ge compound which subsequently transforms to the amorphous alloy with continued milling. A clear example of this behavior was observed in the Nb-Sn system [115]. In such cases first a crystalline compound is found which subsequently transforms to the amorphous alloy with continued milling. Therefore a following sequence of reaction is observed with milling time $A_n + B_m \rightarrow$ Crystalline A_nB_m, which is in effect a variation of first producing the equilibrium intermetallic which can then be amorphized. In order for amorphization to occur by mechanical milling of an equilibrium intermetallic compound, the free energy of the crystalline compound must be raised above that of amorphous phase.

Another interesting feature of mechanical alloying with regard to amorphization is that the glass forming range (GFR), in general, is found to be wider in mechanical alloying than in other amorphization techniques like RSP (rapid solidification process). In the case of RSP, GFR is restricted mainly to the deep eutectic regions due to kinetic constraints. Also glass formation is very difficult by RSP for the compositions corresponding to stable intermetallic compounds and in liquid immiscible system. However, amorphization of intermetallic compounds [109], mixture of intermetallic compounds [116] and liquid immiscible alloys [117] has been achieved by mechanical alloying. Amorphization is also difficult by RSP in systems with shallow

eutectics and cascade of peritectics. Recently, El-Eskandarany et al [118] have shown a GFR of 10-90 at% Ta by mechanical alloying in Al-Ta system, wherein amorphization has not been observed so far by RSP. Incidentally, this is the widest GFR obtained in a binary alloy system by mechanical alloying. Schultz [119] reported a GFR of 35-55 at% Ti in Al-Ti systems. Cocco et al [120] and Bonetti et al [121] also observed the amorphization of $Al_{25}Ti_{75}$ in a Spex mill but they could not amorphize $Al_{75}Ti_{25}$ in their study. Very recently Murty [122] obtained a much wider GFR of 25-90 at% Ti in this system by mechanical alloying in a planetary mill.

Even though amorphization has been reported in many binary alloy systems by mechanical alloying, reports on ternary alloy systems are very few [123-125]. Sundaresan et al [123] were the first to report amorphous phase formation in Ti-Ni-Cu system for the elemental blend of composition $Ti_{72}Ni_{16}Cu_{12}$ using a Spex Mill. Subsequently, Murty et al reported amorphous phase formation for the compositions $Ti_{60}Ni_{40-x}Cu_x$(x = 10, 20, 30) in this system in a planetary mill.

2.3.5 Synthesis of Intermetallics by Mechanical Alloying

As mentioned earlier also mechanical alloying, technique which was originally developed to produce oxide dispersion strengthened nickel and iron-base superalloys, has been effectively used to refine the microstructure of the matrix into the nanometer range [126] and to the synthesis of novel phases including supersaturated solid solutions, crystalline and quasicrystalline intermediate phases and metallic glasses produced from either blended elemental or pre-alloyed powders [127-129]. Besides these attributes, mechanical alloying also has the advantage of not involving melting, allowing alloying of elements with significantly differnet melting points, and it is a process scaleable to commercial sizes. Although several intermetallics are produced by conventional ingot metallurgy techniques, synthesis by the powder metallurgy route (especially

via mechanical alloying) offers potential advantages. Firstly, since mechanical alloying is a solid-state powder processing technique, complex solidification paths can be bypassed and problems associated with the narrow composition ranges of some intermetallics can be minimized. Secondly, mechanical alloying is known to produce nanometer grains in all metallic systems and the room temperature creep deformation rate is several orders of magnitude higher in nanocrystalline materials than in conventional grain-size materials; this can lead to enhanced ambient temperature ductility.

Suryanarayana et al [130] used this technique to produce intermetallics in Ti-Al, Fe-Al and Nb-Al systems with refined (nanostructured) microstructure. In Ti-Al system they observed the following sequence of phase formation with milling time for blended elemental powders:

$(Ti + Al) \rightarrow Ti(Al)_{ss} + Al \rightarrow$ Amorphous $\rightarrow$ fcc

On milling the blended elemental powders corresponding to composition of Ti-48, 50-58 and 60 Al, first a Ti(Al) (hcp) solid solution is formed with some free Al still remaining. Further milling resulted in the formation of amorphous phase which on subsequent milling transformed into the fcc phase. The results obtained on the four different alloy (Ti-48, -50, -55, -60 Al were almost identical to each other. In Fe-Al system, the following sequence of phase formation was observed for Al-25Fe powder.

$$Al + Fe \rightarrow Al(Fe) + Fe \rightarrow Al_5Fe_2 + Al(Fe) \rightarrow Al_5Fe_2 \rightarrow \text{Amorphous}$$

After 5 hours of milling an Al(Fe) solid and some fcc Fe were present. After 15 hrs of milling formation of intermetallic Al_5Fe_2 was observed. After 30 hrs of milling 100% formation of Al_5Fe_2 was observed (instead of Al_3Fe_2) due to some Al loss during milling. Further milling upto 50 hrs resulted in the formation of amorphous phase.

In the iron-rich Fe-Al powders, a supersaturated solid solution of Al in Fe i.e., α-Fe(Al)

was obtained in Fe-25Al powder on milling the blended elemental powders. The crystal size decreased exponentially with milling time and reached nanometer levels. Subsequent heat treatments at different temperatures and cooling at different rates did not produce either the B2 or DO_3 ordering in the as-received condition. With increasing milling times the superlattice lines in the X-ray diffraction patterns eventually disappear resulting in the formation of disordered α-Fe(Al) solid solution. For Nb-75Al, they have reported the formation of Al_3Nb phase on milling the blended elemental powders for 15 hrs which on further milling upto 40 hrs transforms into an amorphous phases. The sequence of phase formation with milling time is reported as following (Al+Nb) → Al(Nb) + Al_3Nb → Al_3Nb → Amorphous.

Fair and Wood [131] were able to produce a mixture of intermetallic FeAl and iron on milling the blended elemental powder corresponding to Fe-25 at% Al composition in a Pilamec vibratory mill. Subsequent heat treatment of the milled powder resulted in the formation of intermetallic Fe_3Al. However the Fe_3Al produced by this technique had the B2 structure and not the equilibrium DO_3 structure.

Oleszak and Shingu [132] carried out the ball milling of Fe-Al powder mixtures containing 10, 20, 30, 40 and 50 at% Al in a conventional horizontal mill with BPR of 100:1 and speed of 90 rev. min^{-1}. For all alloys studied a disordered bcc solid solution was formed by ball milling. A grain size of several nanometer and maximum r.m.s. strain level upto 1% was observed.

2.3.6 Extended Solid Solutions by Mechanical Alloying

Equilibrium solid solubility limits are often exceeded by nonequilibrium processing methods such as rapid solidification. This is also true for mechanical alloying. There are a number of examples of this effect in the literature, but, with the exception of recent work by

Polkin et al [133], no systematic studies have been reported on solid solubility enhancement by mechanical alloying. It was suggested by Schwarz et al [108] that this increased solid solubility could be explained by the metastable equilibrium between the α-Ni fcc solid solution and the Ni-Ti amorphous phase as opposed to the stable equilibrium between α-Ni and Ni_3Ti. A similar result was obtained by Lee and Koch [134] in a study of amorphization of Ni-Nb alloys by mechanical alloying. The terminal Ni fcc solid solution and the Nb bcc solid solution were found to be approximately 10 at% Nb and 10 at% Ni respectively. This may be compared with solubility limits of 4.2 at% Nb (at 987°C) and 3.5 at% Ni (at 1000°C). The solubility limits at the milling temperature (nominally 60°C) are expected to be much lower.

Hellstern et al [113] found an extended solid solubility of Al in bcc Nb of about 30 at% for mechanical alloying of elemental Nb and Al powder. The stable equilibrium diagram for Al-Nb indicates Al solubility of < 10 at% for temperatures below 1000°C. Similar to the above Ni-Ti and Ni-Nb systems, metastable equilibrium between the bcc solid solution and an amorphous phase at Nb-50 at% Al is apparently responsible for the extended solid solubility. Oehring and Bormann [135] have subsequently shown that ball milling the A15 structure Nb_3Al intermetallic transforms it to the Nb(Al) bcc solid solution.

Ivanov et al [136] obtained a solid solubility of about 27 at% Al in fcc Ni by mechanical alloying of elemental Ni and Al powders. The equilibrium solid solubility of Al in Ni at 500°C is about 4 at%. Again, the metastable fcc solid solution with extended Al solubility is in metastable equilibrium with an amorphous phase found by Ivanov et al. over the composition range of 27 to 35 at% Al.

The equilibrium solubility of Fe in Al is nil ($<3\times10^{-3}$ at%) below 500°C. However, Shingu and coworkers [98,100] have observed an amorphous phase for the composition range

17 to 33 at% Fe in mechanical alloying Al-Fe alloys along with an extended solid solution of Fe in Al upto about 10 at% Fe. Thus, large extended solubility is again associated with the formation of a metastable amorphous phase. Polkin et al [133], have been systematically studying extended solid solutions by mechanical alloying in several systems such as Al-Fe, Ni-Al, Ni-W, and Ni-Cr. Large extensions of solid solubility are seen in these studies. Recently Frattini et al [137] obtained extended solid solutions with the bcc structure by mechanical alloying of pure iron and aluminium powders in the atomic ratio $Fe_{50}Al_{50}$ and $Fe_{75}Al_{25}$.

Sundaresan and Froes [138] have carried out mechanical alloying on the immiscible system Ti-Mg. The solubility of Mg in Ti reported from studies of the phase equilibrium is <0.2 at% for temperatures $\leq$ 700°C. However, Sundaresan and Froes reported solid solubilities for mechanical alloying powder of up to 6.0 at% Mg. No amorphous phase was reported in mechanical alloying of this system. Gaffet and Gaspart [139] have recently reported some mutual solid solubility induced in the immiscible Cu-W system by mechanical alloying. Preliminary X-ray diffraction studies show lattice parameter changes that suggest extended solid solubilities along with the possibility of partial amorphization.

CHAPTER - 3

EXPERIMENTAL PROCEDURE

3.1 RAW MATERIALS

Elemental powders of Fe and Al were used as raw materials for the experiments.

Electrolytic iron powder with purity >99.0% was supplied by Sudhakar Products, Bombay with the following chemical analysis:

Fe min	=	99.00%
C	=	0.025%
S	=	0.02%
H_2 loss	=	0.5%
Other impurities	=	0.11%

The sieve analysis as provided by the suppliers is -

Mesh Analysis	% Retention on Tyler Sieves
+200	40
+325	30
-325	30

Atomized Aluminium powder with purity >99.9% was supplied by Metal Powder Company Ltd., Madurai, Tamil Nadu.

SEM micrographs of the elemental Fe and Al powders is shown in Fig. (3.1).

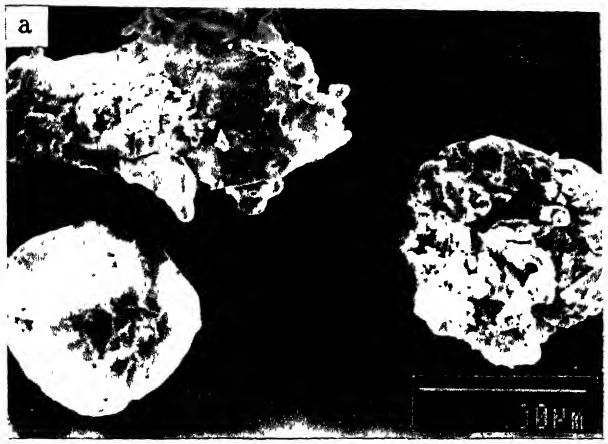

Fig. 3.1 SEM micrographs of elemental (a) Fe and (b) Al powders

3.2 MECHANICAL ALLOYING

Iron and aluminium powders were blended together to the total charge weight of 800g in the ratio of 7:3 by weight (corresponding to Fe-47 at. % Al) and were milled in a T.C. attritor (Torrance, U.K.). The schematic of the attritor is shown in Fig (2.4). The grinding medium was tungsten carbide balls of diameter 9 mm. The ball to powder weight ratio was kept at 10:1 and the milling was carried out at the speed of 500 r.p.m.

The mill had a water cooling arrangement to minimize the temperature rise of the powder during milling. Toluene was used as a process controlling agent to prevent excessive welding of the particles during milling. To follow the progress of mechanical alloying during milling, small quantities were withdrawn from the mill after the milling times of 15 min, 30 min, 45 min, 1 hr, 2 hrs, 3 hrs, 5 hrs, 10 hrs, 15 hrs, 20 hrs, 40 hrs, 60 hrs, 80 hrs, 100 hrs, 120 hrs, 150 hrs, 185 hrs, 200 hrs and 235 hrs.

3.3 CONSOLIDATION OF MECHANICALLY ALLOYED POWDER

Fe-47 at. % Al powder mixture milled for 235 hrs was consolidated using hot pressing technique. Hot press of Dr. Fitsch, K.G., west Germany make was used for this purpose. The dies and punches used for hot pressing were made of graphite. Dies were typically of 30 mm height having a through hole of 8 mm diameter and a small blind hole of 3 mm diameter (3 mm depth) to accommodate thermocouple. Twin punches of 15 mm height and 8 mm diameter were used. Prior to hot pressing, dies and punches were dip coated with a thin layer of BN, where they would come in contact with premixed powder. The pressing was carried out at different temperatures varying from 600°C to 1100°C under a constant applied pressure of 20 MPa. At a given temperature, holding time of 5 to 20 minutes was given. The requisite temperatures were obtained by resistance heating of graphite dies. The temperature was continuously

monitored by a chromel alumel thermocouple inserted into the graphite die wall. (A schematic sketch depicting the hot press set-up is shown in Fig. (3.2)).

3.4 ORDERING TREATMENT

The hot pressed compacts of mechanically alloyed powder were encapsulated in quartz glass tube under normal vacuum and given ordering treatment at 1000°C for durations of 6 hrs, 12 hrs, 18 hrs, 24 hrs and 48 hrs.

3.5 CHARACTERIZATION METHODS

3.5.1 X-ray Diffraction

Powder samples, taken out of the attritor mill after different milling times ranging from 15 min to 235 hrs, and compacts prepared by hot pressing of MA powder were characterized using X-ray diffraction technique. The instrument used was Scifert, ISO-DEBYFLEX 2002 diffractometer with copper target. The tube was operated at 30 kV and 10 mA. The radiation used was CuK_{α} having wavelength of 1.540598 Å .

From the XRD patterns obtained, d- values were calculated using the Braggs formula

$$\lambda = 2d \sin \theta$$

The d- values so obtained were compared with standard d-values given in JCPDS Powder Diffraction files to identify the phases.

The crystallite size and rms strain of the mechanically alloyed were calculated from the observed broadening of difraction lines in X-ray difraction patterns.

To separate the effect of crystallite size reduction from that of lattice distortion, the approach of Williamson and Hall was adopted.

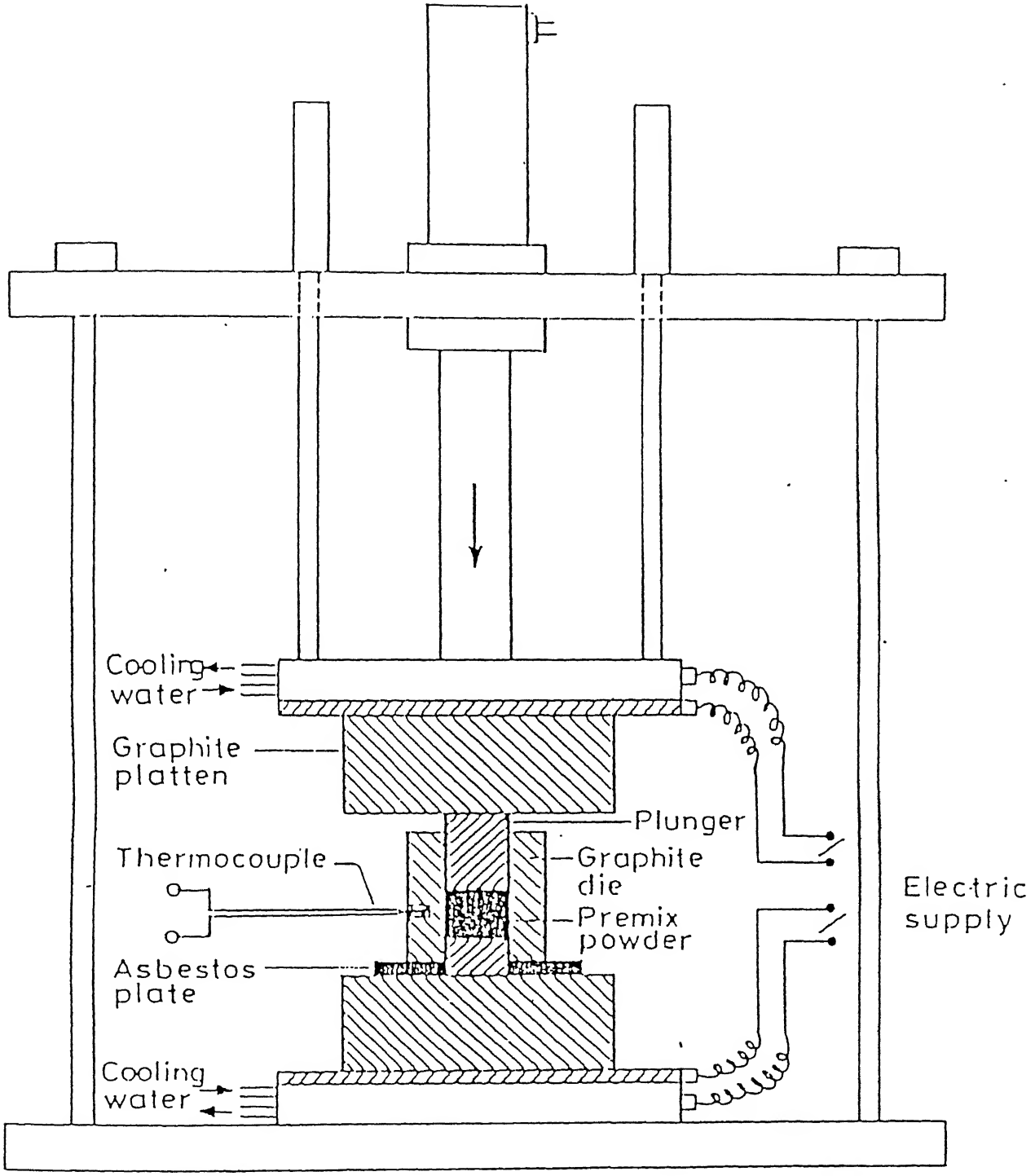

Fig. 3.2 Schematic of hot press set-up

The strain e in a crystal lattice produce some broadening β_e of the diffraction lines:

$$\beta_e = 2A \langle e^2 \rangle^{1/2} \tan \theta$$

where θ is the Bragg angle, A is a coefficient which depends on the distribution of strains and close to unity for dislocations, and $\langle e^2 \rangle^{1/2}$ is the r.m.s. strain.

The broadening resulting from small crystallite size is given by the Scherrer relationship

$$\beta_D = \frac{K\lambda}{D \cos \theta}$$

where λ is the X-ray wavelength, K is the Scherrer constant, D is the crystallite size and θ is the Bragg angle.

It is possible to separate the two effects by plotting experimentally measured broadening B cos θ / λ against sin θ / λ , when the intercept gives a measure of D and the slope $\langle e^2 \rangle^{1/2}$.

3.5.2 Scanning Electron Microscopy

Powder samples withdrawn from the mill at different time intervals were hot mounted for microscopic examinations of sections of powders. These mounted powder samples and compacts of hot-pressed MA powder were observed by JEOL JSM 840 A Scanning Electron Microscope (SEM) using an operating voltage of 15-20 kV.

Back scattered images were taken to obtain the distribution of elements in the samples and reveal the presence of characteristic layered structure in the early stages of MA. Qualitative EDX analysis facility was used to detect the presence of different elements.

3.5.3 Electron Probe Microanalysis

For obtaining accurate elemental analysis of mechanically alloyed powder samples and hot pressed compacts of MA powder, electron probe microanalysis (EPMA) technique has been used. In this microanalysis, a small electric probe ($\sim$100 nm diameter) is used to generate X-rays from a defined area of a polished specimen and the intensity of the various characteristic x-rays measured using wavelength dispersive spectrum spectrometer (WDS). Typically the accuracy of the analysis is $\pm 0.1\%$.

3.5.4 Hardness Testing

Hardness of hot pressed compacts were measured using Rockwell hardness tester on the C scale using a 150 kg major load.

3.5.5 Compression Testing

Compression tests were carried out using an INSTRON machine. Full scale load used was 100 KN. The compressive strength were calculated from the load applied divided by the initial area of compaction.

CHAPTER - 4

RESULTS AND DISCUSSIONS

4.1 PREPARATION OF MECHANICALLY ALLOYED POWDERS

4.1.1 Effect of Milling Time on the Process of Mechanical Alloying

The progress of Mechanical Alloying between Fe and Al powders was investigated in the present study through X-ray diffraction studies. For this purpose, powder samples were taken out from the mill after milling times of 15 min, 30 min, 45 min, 1 hr, 1 hr 30 min, 2 hrs,3 hrs, 5 hrs, 10 hrs, 15 hrs, 20 hrs, 30 hrs, 40 hrs, 50 hrs, 60 hrs, 80 hrs, 100 hrs, 120 hrs, 150 hrs, 185 hrs, 200 hrs and 235 hrs.

As mentioned earlier, Mechanical Alloying is a solid state powder processing technique which involves high energy milling of blended elemental powder mixture to form alloy. By X-ray diffraction technique the process of mechanical alloying in any system is monitored through presence of elemental peaks in X-ray diffraction patterns of milled powder samples. The mechanical alloying is understood to have completed when no elemental peaks can be detected in the X-ray diffraction patterns of the milled powders.

A comparison of standard powder diffraction data for elemental Fe and elemental Al (Table 4.1) reveals that reflections from elemental Fe are too close to the reflections from elemental Al to be revealed separately. Therefore the presence of elemental Fe cannot be unambiguously ascertained through X-ray diffraction patterns in Fe-Al system. However, the reflection Al (111) which is the strongest reflection from elemental Al does not overlap with any of the reflections from Fe, and Al (322) too is a non-overlapping reflection. It was therefore decided to consider these two reflections as the reference to monitor the changes occurring during the process of mechanical alloying. The X-ray diffraction patterns typically obtained

Table 4.1

Standard d and 2θ Values for Elemental Iron and Aluminium

Element	d	2θ	Intensity	h k l
Fe	2.03	44.67	100	110
	1.43	65.02	20	200
	1.17	82.34	30	211
Al	2.34	38.47	100	111
	2.02	44.74	47	200
	1.43	65.14	22	220
	1.22	78.23	24	311
	1.16	82.44	7	222

after milling times of 15 min, 30 hrs, 40 hrs and 235 hrs are shown in Fig. (4.1).

As can be seen from Fig. (4.1), the intensity of Al (111) reflection is very strong in X-ray diffraction pattern of sample milled for 15 min. However with increase in milling time, it is observed, that the intensity of Al(111) reflection gets weakened. The intensity becomes very weak after 30 hrs of milling and finally it becomes invisible for a milling time of 40 hrs.

It has been discussed in Chapter 2.4 that the process of mechanical alloying during high energy milling of elemental powders, occurs due to repeated cold welding and fracturing of flattened/semi-flattened particles. Elemental particles which to start with, are present as individual particles became composite particles and loose their individual identity as milling time increases. Composites particles subsequently transform into mechanically alloyed powder particles.

In order to identify the product formed after mechanical alloying, the X-ray diffraction patterns were subjected to further analysis. In addition to a wide range of solid solution of Al in Fe (upto 22 at% Al) a number of intermetallic compounds namely Fe_3Al, FeAl, $FeAl_2$, Fe_2Al_5 and $FeAl_3$ are reported in the Fe-Al system. The standard X-ray diffraction data for these intermetallic compounds is shown in Table (4.2). As it can be seen from these data that the fundamental peak positions belonging to these intermetallic compounds are very close to those of elemental Fe and Al powders and therefore are difficult to be resolved separately. Therefore, the presence of these ordered intermetallic compounds can be detected only through the presence of superlattice reflections. The analysis of X-ray diffraction patterns, in the present investigation, does not indicate the presence of any superlattice reflections belonging to these ordered intermetallics.

Further analysis of X-ray diffraction patterns as obtained from the milled powder samples

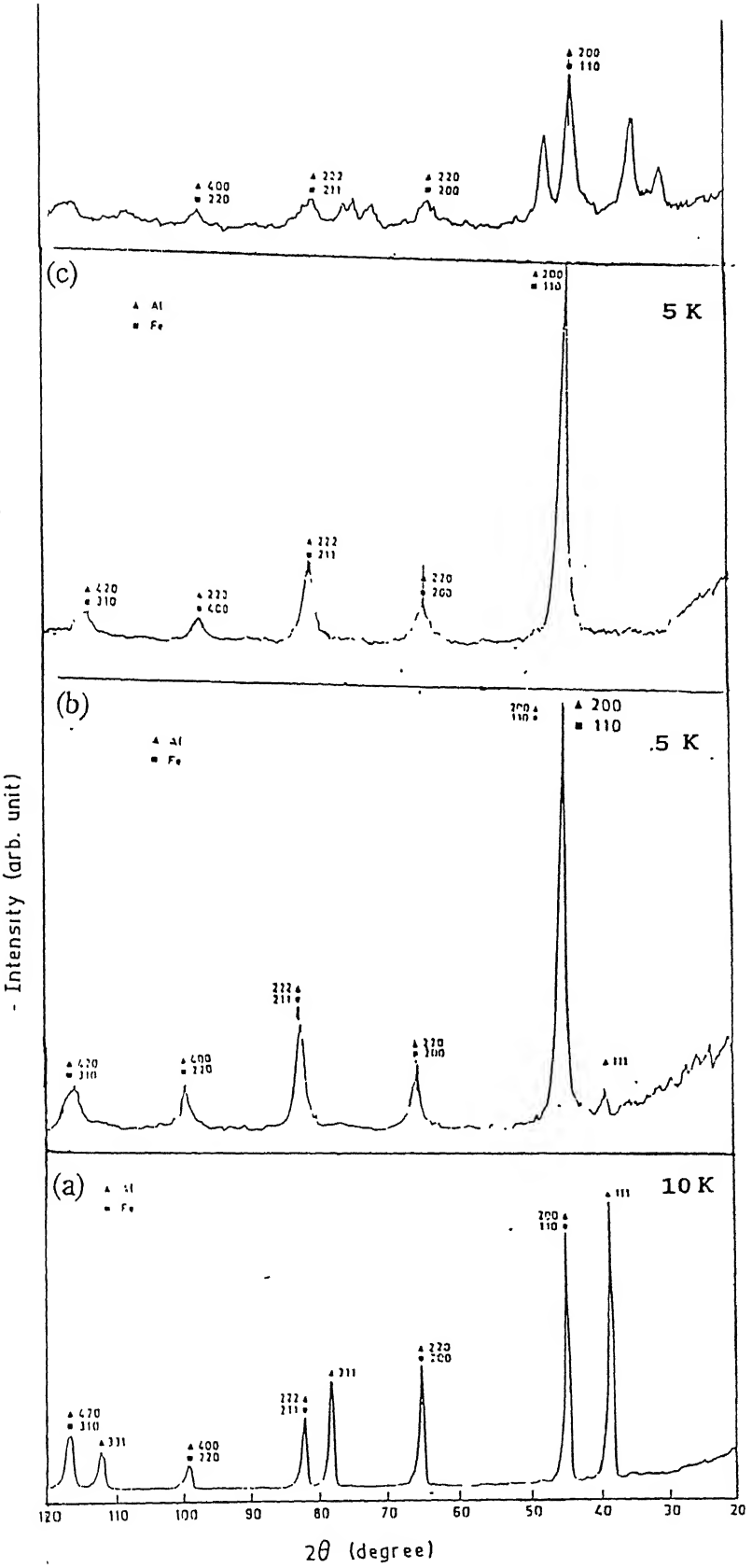

Fig. 4.1 X-ray diffraction patterns of blended elemental Fe-47 at% Al powder after milling times of (a) 15 min (b) 30 hrs (c) 40 hrs and (e) 235 hrs.

Table 4.2

Standard d Values for Different Fe-Al Intermetallics

Intermetallic Compound	d	Intensity	h k l
FeAl	2.05	100	110
	1.18	25	211
	1.45	14	200
Fe_3Al	2.04	100	220
	1.18	90	420
	1.45	80	400
Al_5Fe_2	2.11	100	002
	2.05	100	130
	3.2	40	020
Al_2Fe	4.67	100	-111
	4.23	80	640
	3.65	80	1-31
$Al_{13}Fe_4$	2.10	100	-623
	2.05	85	025
	2.04	83	423

revealed that the corresponding b.c.c. Fe peaks get slightly broadened with milling time. In addition to the broadening of these peaks a little shift in the peak positions was also observed. However the shift was pronounced only for higher milling times. The peak shift was attributed to an increase in the lattice parameter of b.c.c. iron due to alloying with aluminium which has a larger atomic size.

These observations led to the conclusion that the mechanical alloying of Fe-47 at% Al powder mixture, for 235 hours, leads to the formation of disordered b.c.c. solid solution of aluminium in iron and not the ordered intermetallic phases.

Similar results were obtained by Olezak et al [132], Frattini et al [137] and Suryanarayan et al [130]. In earlier studies on mechanical alloying in the Fe-Al system, Olezak et al carried out the milling of Fe-Al powder mixtures containing 10, 20, 30, 40 and 50 at % Al in a conventional horizontal low energy ball mill with ball to powder ratio of 10:1 and speed of 90 rev. min^{-1}. For all alloys a disordered b.c.c. solid solution was formed. For Fe-50 at% Al, diffraction peaks corresponding to the planes of f.c.c. became weak with increasing milling time and were almost negligible after 100 hours of milling. Frattini et al also reported the formation of extended b.c.c. solid solution on milling Fe and Al powders corresponding to $Fe_{50}Al_{50}$ and $Fe_{25}Al_{25}$ compositions. Suryanaryana et al obtained a supersaturated solution of Al in Fe after 10 hours of milling. However, in Al rich side, for Al-25 at% Fe they have reported the formation of Al(Fe) solid solution after 5 hours of milling which on further milling transforms into intermetallic Al_5Fe_2. 100% Al_5Fe_2 was observed after 30 hours of milling. Further milling resulted in amorphization and full amorphization was observed after 50 hours of milling.

In the present investigation milling of the powder was carried upto 235 hours to see if any amorphization could be achieved. Occurrence of amorphization is generally detected in

XRD pattern by substantial broadening of the peaks. However, as mentioned earlier also analysis of the XRD patterns of the milled powders revealed only slight broadening and no substantial broadening was detected. Therefore it was concluded that no amorphization has occurred in the powder milled for 235 hours.

4.1.2 Effect of Milling Time on the Size and Morphology of Powders Prepared

Fig. 4.2 shows the SEM micrographs of the powder samples after milling times of (a) 15 minutes (b) 45 minutes (c) 3 hours (d) 5 hours and (e) 40 hours. A quantitative examination of micrographs reveals that the average particle size of powder milled for 45 min is greater than that of powder milled for 15 minutes. However the particle size of the powder milled for 3 hours is found to be less than that of powder milled for 45 minutes. Therefore it can be inferred that initially the size of the powder particle increases with milling time upto, say, 45 min but however, it starts decreasing between milling times of 45 minutes and 3 hours. Further from Fig. 4.2(d) and Fig. 4.2 (e) which show the SEM micrographs of powder milled for 5 hours and 40 hours respectively, it can be seen that with further increase in milling time the particle size decreases further.

A comparison of the SEM micrographs of powder samples milled for 15 min, 45 min, 3 hours and 5 hours. (Fig. 3.1) reveals that the morphology of powders remains more or less same as that of starting elemental powders upto this time of milling. As in elemental powders, significant variability in morphology can still be seen in powders upto this time of milling. However, after a longer time (Fig. 4.2(e)) it is observed that the particles get more regular and spherical in shape.

Fig. (4.3) shows the SEM micrographs of the powder after milling time of 15 min and 45 min. The micrographs show particles in a deformed and flattened state. It is also observed

Fig. 4.2 SEM micrographs of blended elemental Fe-47 at% Al powder after milling times of (a) 15 min (b) 45 min (c) 3 hrs (d) 5 hrs and (e) 40 hrs.

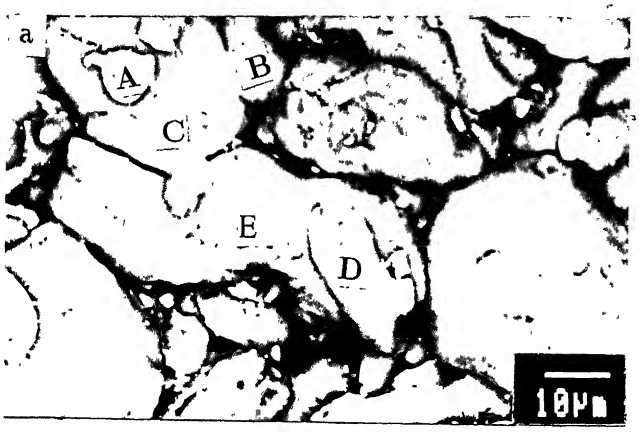

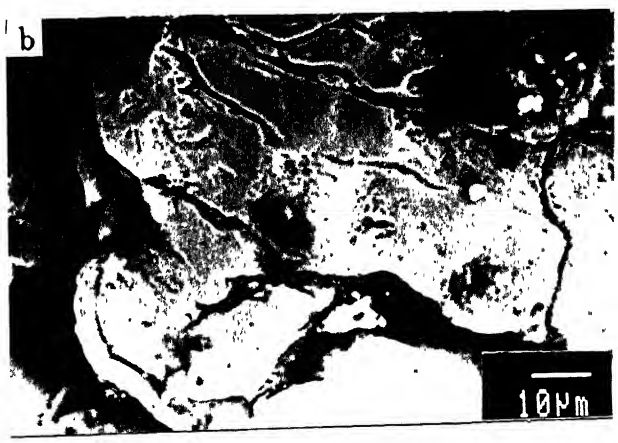

Fig. 4.3 SEM micrographs of powder after milling times of (a) 15 min (b) 45 min

that some of the particles have got welded to each other. From Fig. 4.3(a) we can see particles "A" and "B" welded to the particle "C" and particle "D" welded to the particle "E". Similarly welding of particle "C" with "E" can also be seen in the micrographs.

In mechanical alloying process the particles are repeatedly deformed, fractured and rewelded. Every time two balls collide they trap powder particles between them. The force of the impact deforms the particles and creates atomically new surfaces. When the clean surfaces come in contact they weld together.

Micrograph of the powder sample milled for 45 min, Fig. 4.3(b), shows a composite particle. Aluminium particle (dark gray) sandwiched between iron/iron solid solution particles (light gray) can be seen in the micrograph. Qualitative EDS analysis revealed that dark gray region was Al-rich while the light gray region was Fe-rich.

Another important feature which can be revealed in the 45 min milled powders particles is the characteristic layered structure in the composite particle (Fig. 4.4). Alternate layers of iron and aluminium in the powder particle can be seen in the micrographs. At initial stages of mechanical alloying the metal powder particles are still soft, and the tendency for them to weld together predominates. Repeated deformation and welding of elemental particles results in the formation of such composite particles containing layers of the alloy component.

4.1.3 Effect of Milling Time on Crystallite Size and R.M.S. Strain

Analysis of the X-ray diffraction patterns of the powder samples, milled for different durations of time, reveals that the peaks get slightly broadened with increasing time. This observed broadening of the diffraction can be attributed to the refinement of the crystal size and an increase in internal strains during milling.

Figure (4.5) and Figure (4.6) show the dependance of the calculated crystallite size and

CENTRAL LIBRARY
I. I. T., KANPUR
No. A 128041

powder after milling time of 45 min

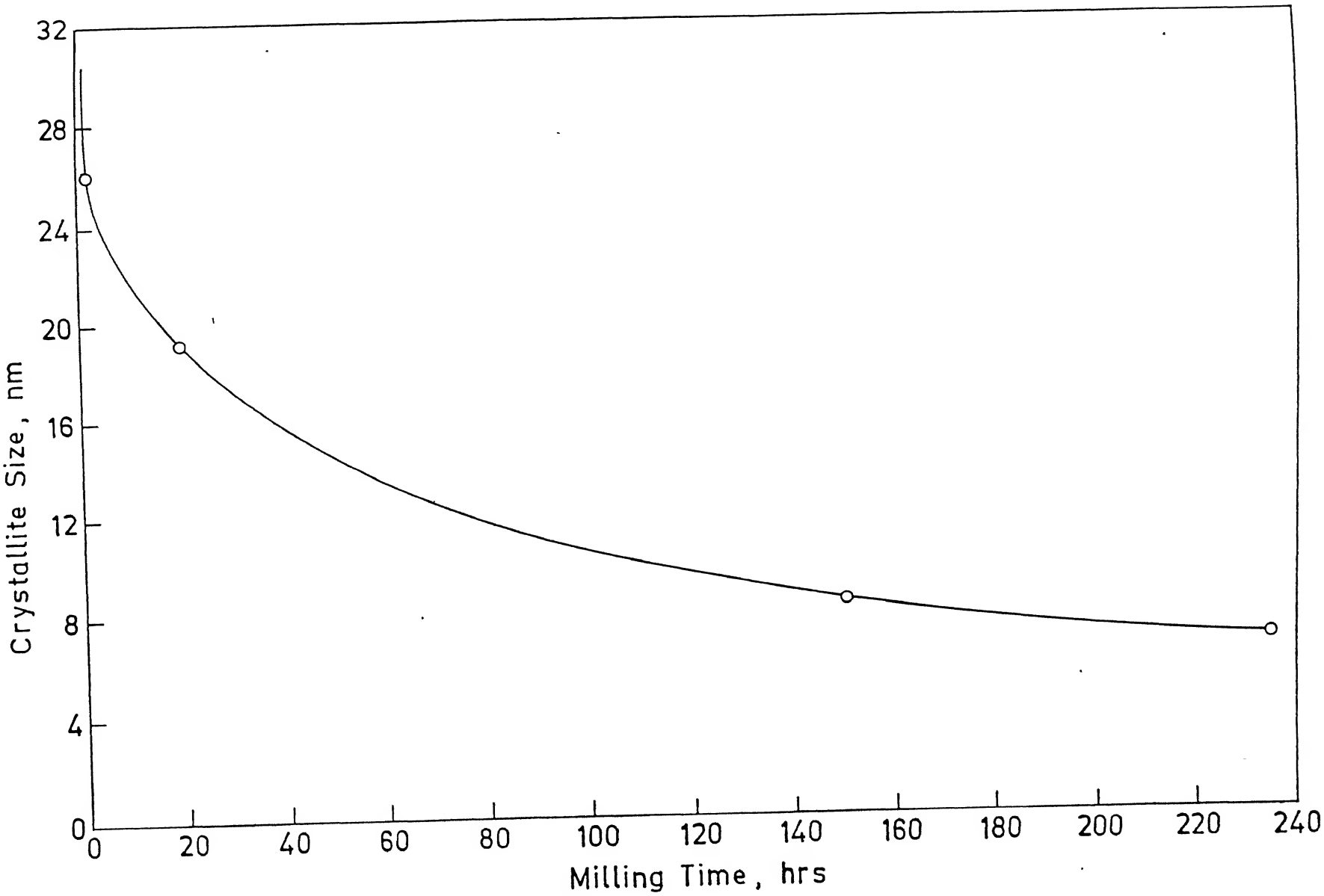

Fig. 4.5 Crystallite Size vs. Milling Time.

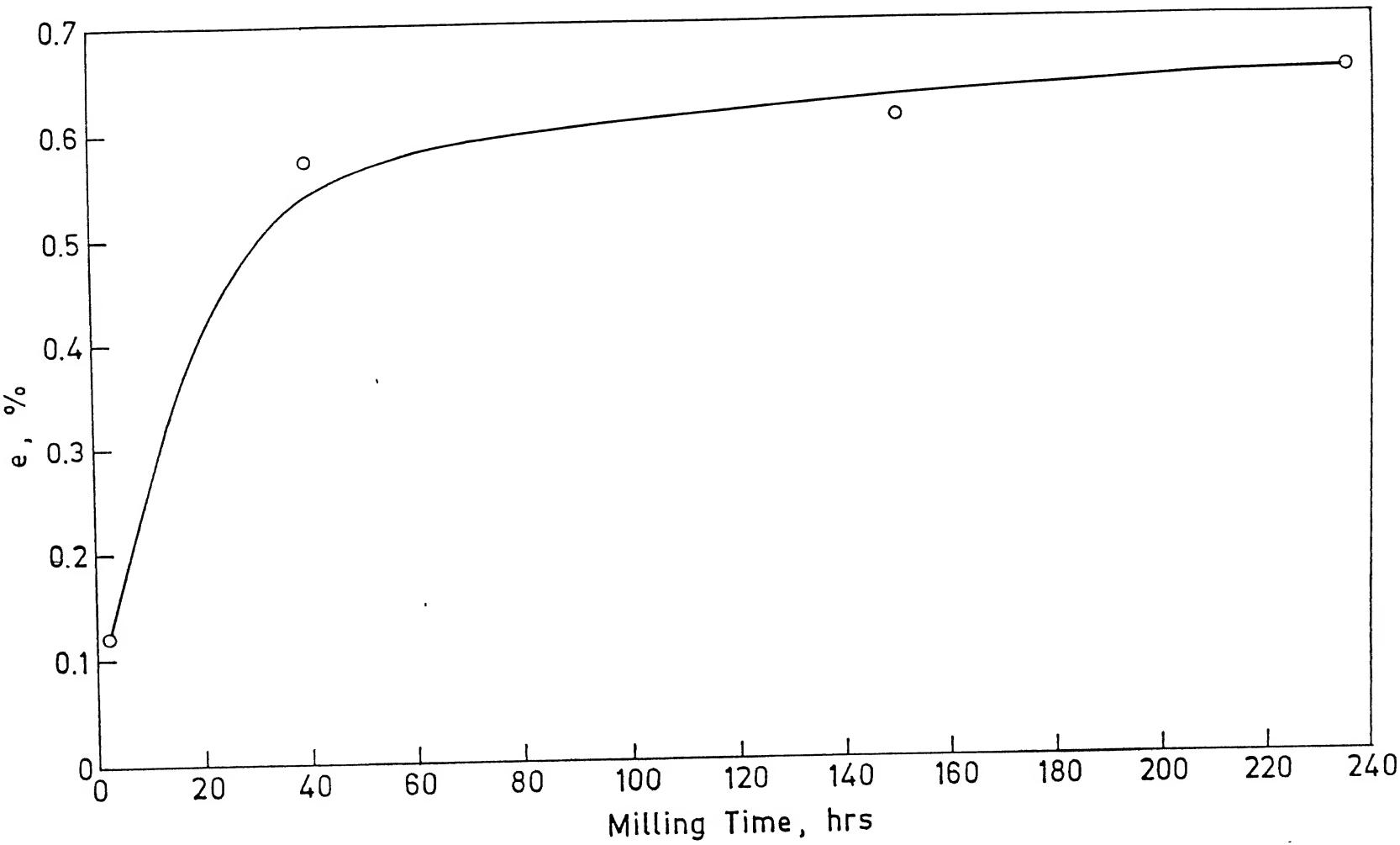

Fig. 4.6 R.M.S. Strain vs. Milling Time.

r.m.s. strain on milling time. The rate of refinement of crystallite size is faster in the early stages of milling but gradually decreases as the milling time increases. The crystallite size obtained after 235 hrs of milling of Fe-47 at% Al powder mixture is 7nm. R.M.S. strain is found to increase with increase in milling time. The rate of increase is faster in the early stage of milling but becomes very slow after long hours of milling. The final value of r.m.s. strain obtained after 235 hours of milling is 0.65%.

This is in agreement with the previous studies done on mechanical alloying of elemental powders. Suryanarayana et al [130] obtained crystals of about 10 nm size after 30 hrs of milling of blended elemental powders mixture of Fe and Al corresponding to composition of Fe-25 at% Al. The milling was carried out in a Spex 8000 Shaker mill with ball to powder ratio of 1-:1. Olezak et al [132] obtained grain sizes of 4 nm and 8 nm for Fe-50 at% Al and Fe-10 at% Al respectively after 600 hours of milling in a conventional low energy ball mill. For R.M.S. strain they have reported that it first increases with milling time, reaches a maximum value and then decreases upon further milling. In the present investigation R.M.S. strain increases with milling time and reaches a maximum value of 0.65% after 235 hours of milling.

Frattini et al [137] have also reported formation of crystals in nanometer range of bcc solid solution for Fe-25 at% Al and Fe-50 at% Al.

4.1.4 Effect of Milling Time on Lattice Parameter

Analysis of the X-ray diffraction patterns of the milled powder samples show that the diffraction lines corresponding to bcc α-Fe overlap those for fcc Al and shift to the low angle size with increasing milling time. This can be attributed to the increase in lattice parameter of the bcc Fe with increasing mechanical alloying time. This result clearly testifies that aluminium atoms, which have a larger atomic radius than iron atoms, dissolve in iron, thereby forming a

solid solution of Al in Fe.

The changes in lattice parameter have been measured from the shift of the (211) diffraction line. The lattice parameter value of 2.872Å is obtained after 235 hrs. of mechanical alloying for Fe-47 at% Al powder sample. This value corresponds to a 0.7% change in lattice parameter. The trends of change in lattice parameter are well established and have been observed during the mechanical alloying of Fe-Al system also. Results of Olezak et al [132] indicate a change of ~0.9% in lattice parameter of bcc α-Fe, for a milling time period of 235 hours for Fe-50 at% Al. They observed a 2.4% change in lattice parameter of the bcc Fe after 600 hours of mechanical alloying of Fe-50at% Al powder mixture. They reported saturation value of 2.935Å after 600 hours of mechanical alloying. Frattini et al [137] obtained the value of 2.903Å after 30 hours of mechanical alloying in wet milling i.e., in presence of ethanol as a lubricant. In dry milling condition i.e., in absence of ethanol they noticed a significant change in lattice parameter, from 2.865Å for pure Fe to 2.912Å, in a much smaller milling time of only 8 hours. It is, therefore, understood that the process control reagents (sometimes quoted as lubricant also) significantly affects the changes in lattice parameter. Their presence shows down the diffusion of Al into the bcc lattice of Fe and thereby causing a slower change in lattice parameter. The slower decrease in lattice parameters, as observed in the present study, can be attributed to the presence of process control reagent i.e. toluene.

4.1.5 Effect of Milling Time on Theoretical Density

From the binary phase diagram of Iron and Aluminium it can be seen that Fe-47 at. % Al composition lies in the B2 single phase region at room temperature. B2 is an ordered structure having two interpenetrating simple cubic lattices with the atoms of each constituent at the body centre of the other. The Fe-Al B2 structure has a lattice parameter of 2.90 Å. The

density of stoichiometric FeAl ordered phase is 5.6 g/cm^3.

In the present investigation the milling of Fe-47 at. % Al powder mixture for 235 hrs has resulted in the formation of a disordered bcc solid solution. The lattice parameter value of this disordered solid solution has been found to be 2.872 Å.

Using this value of lattice parameter theoretical density of the milled powder sample has been calculated. The value obtained is 5.882 g/cm^3.

4.2 HOT PRESSING OF MECHANICALLY ALLOYED POWDERS

4.2.1 Effect of Hot Pressing Temperature on the Densification of the Mechanically alloyed Powder

The milled powder samples were consolidated using hot pressing technique at different temperatures at a constant pressure of 20 MPa and constant holding time of 5 minutes. Fig. (4.7) shows the variation of % densification of the hot pressed compacts as a function of hot pressing temperature.

It was observed that % densification increased with increasing temperature. A maximum densification of nearly 95% was obtained at a hot pressing temperature of 1100°C. This shows that hot pressing can be a viable processing technique for consolidating mechanically alloyed powders.

4.2.2 Effect of Hot Pressing Time on the Densification of the MA Powder

Fig. (4.8) shows the variation of % densification as a function of hot pressing time at a temperature of 1000°C and applied pressure of 20 MPa. % Densification increases with increasing holding time. Maximum densification of 95% is observed for a holding time of 20 min.

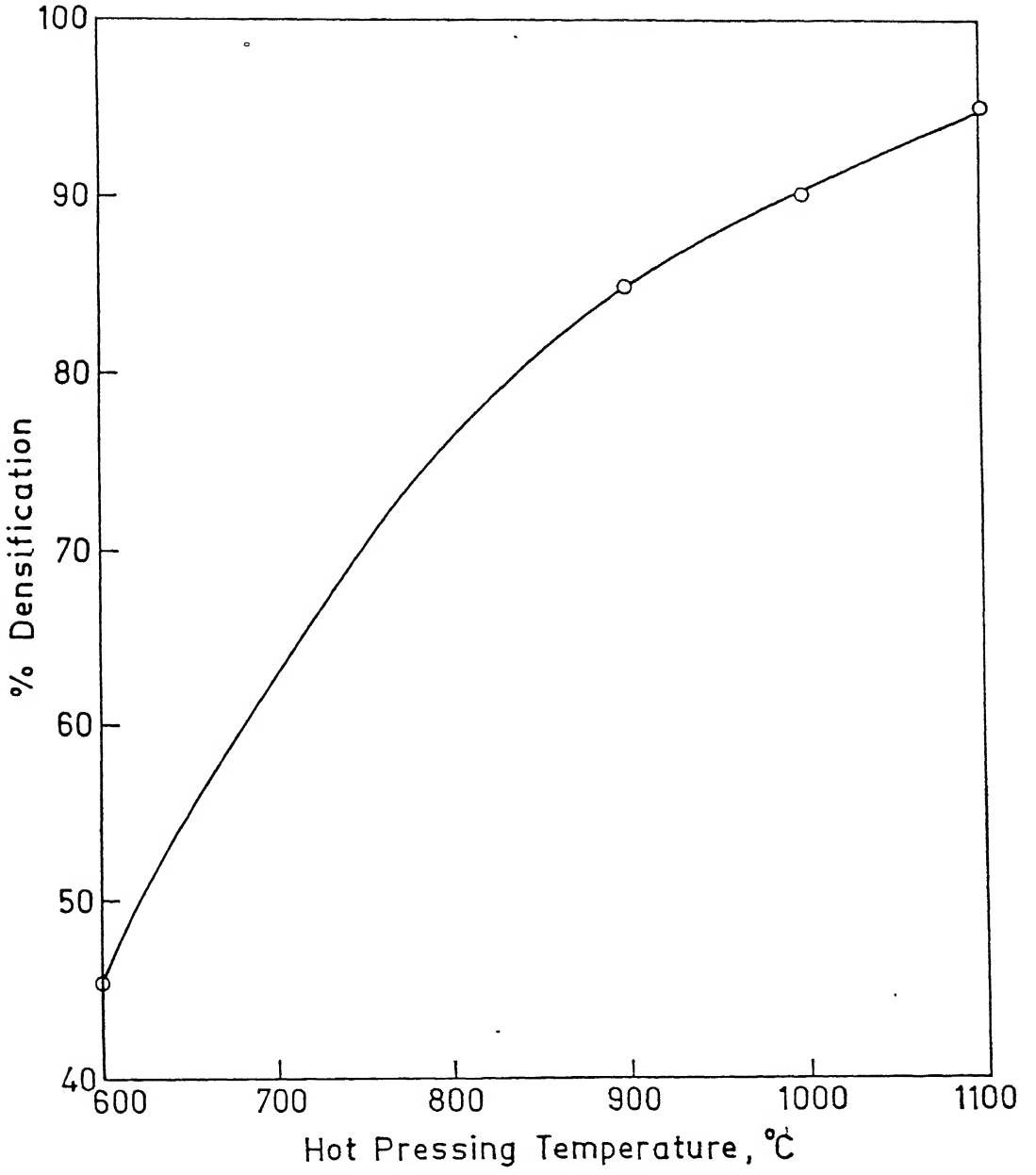

Fig. 4.7 % Densification vs. Hot Pressing Temperature.

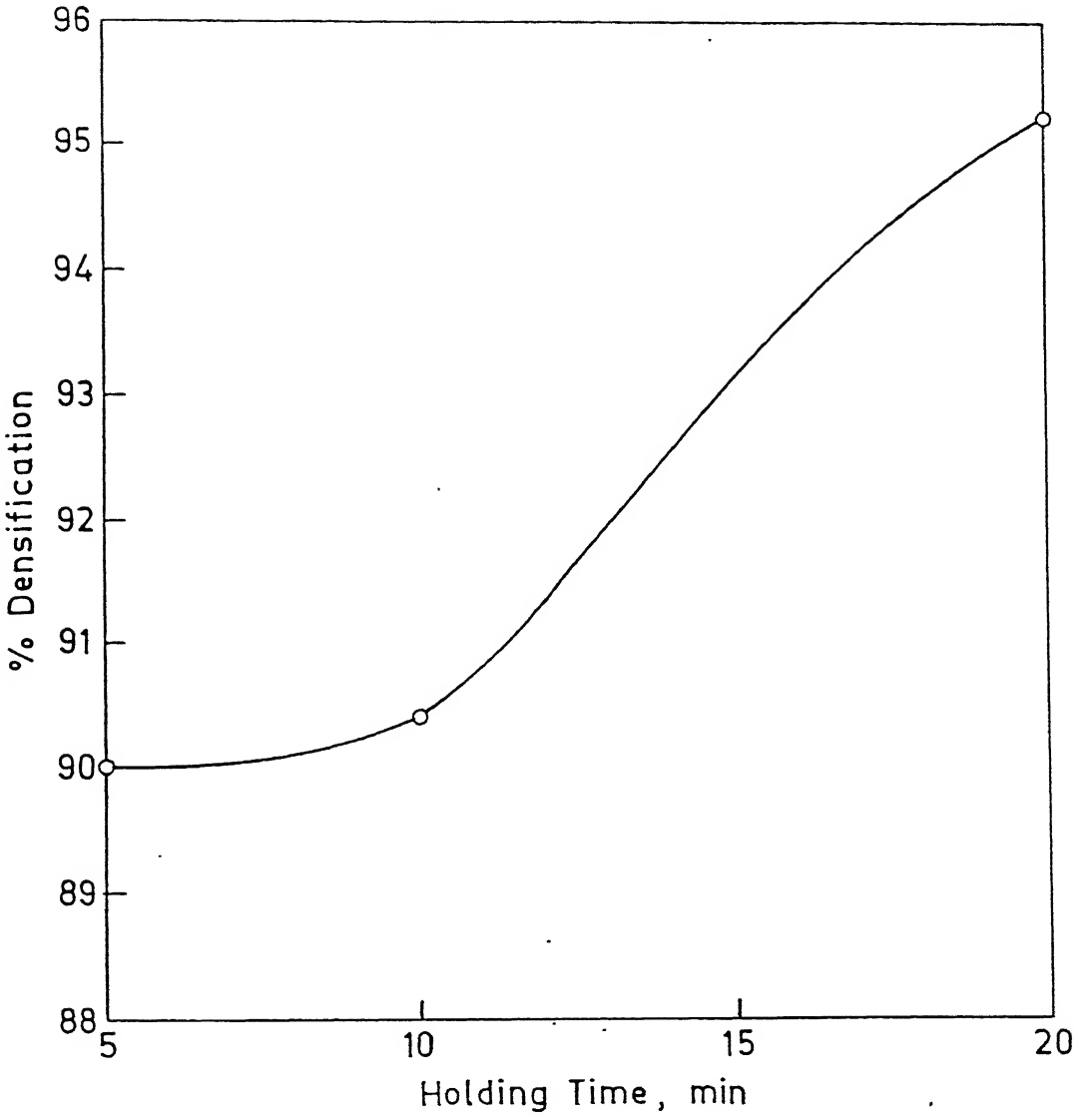

Fig. 4.8 % Densification vs. Holding Time.

4.2.3 Microstructural Features of Hot Pressed Compacts

Fig. (4.9) shows the micrographs of the powder samples hot pressed at three different temperatures (a) 900°C, (b) 1000°C and (c) 1100°C. Two distinct regions can be seen in the micrographs - black regions and white regions. Qualitative EDS analysis of the samples revealed that the black regions in the micrograph were Al-rich while the white regions were Fe-rich.

4.2.4 Occurrence of Grain Growth and Other Structural Changes During Hot Pressing

The crystallite size of the powder sample hot pressed at a temperature of 1000°C, under a pressure of 20 MPa and holding time of 20 min, was calculated from the observed broadening of the diffraction lines in the X-ray diffraction of the hot pressed compact. The crystallite size was found to be 35 m. The crystallite size of the unconsolidated powder sample was calculated to be 7 nm. This shows that some grain growth has taken place during hot pressing but, however, the crystallite size remains in the nanometer range.

4.2.5 Hardness and Compressive Strength of Hot Pressed Compacts

The hardness of the compact hot pressed at a temperature of 1000°C, for a holding time of 20 min was found to be $49R_c$. The compact had nearly 95% densification.

Compression testing of the compact hot pressed at 1000°C for a holding of 20 min. showed that the compact fractured at a stress of 1.37GPa.

4.2.6 Structural Changes During Ordering Treatment

From the analysis of the X-ray diffraction patterns of the compacts, which were given ordering treatment at 1000°C for time periods of 9 hrs, 15 hrs, 24 hrs respectively, it appears that some transformation of the structure from predominantly solid solution to that of ordered structure begins. Several peaks were detected in the X-ray diffraction patterns. However, due to lack of more results and insufficient data in the literature, they could not be clearly discerned.

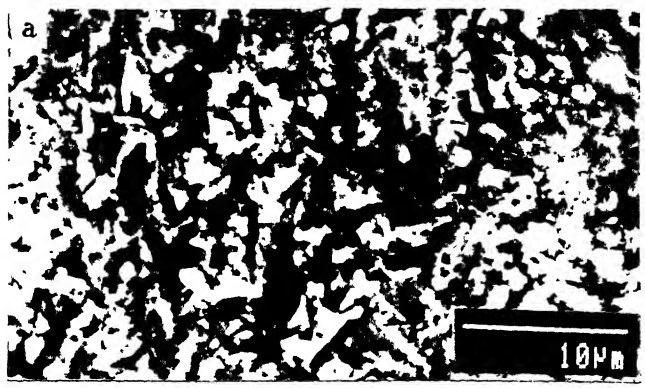

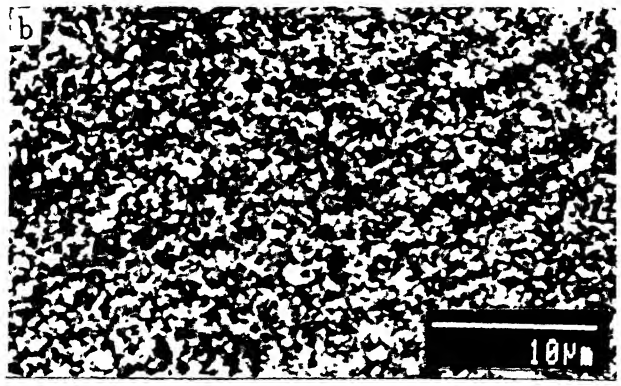

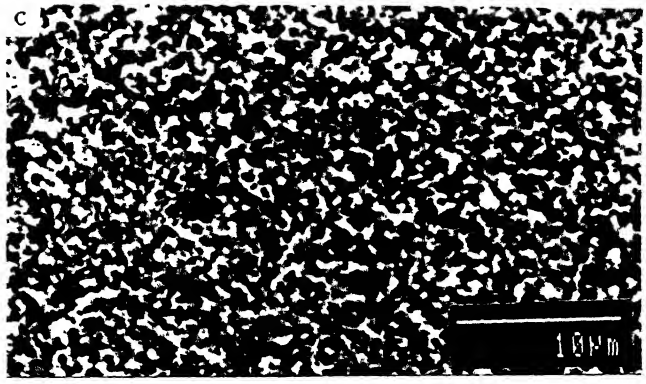

Fig. 4.9 SEM Micrographs of Mechanically alloyed powder samples hot pressed

CHAPTER - 5

CONCLUSION

Based on the results obtained by preparing mechanically alloyed Fe-47 at. % Al powder and its further processing the following conclusions can be made.

1. Mechanical alloying appears to be a viable method for preparing mechanically alloyed Fe-47 at. % Al powder. However, mechanical alloying of Fe-47 at. % Al powder for 235 hrs results in the formation of supersaturated solid solution of Al in Fe and no intermetallic compound formed during the course of milling. Similarly, no amorphization could be achieved by milling upto 235 hrs.
2. Refinement of the crystallite size occurs to the nanometer dimension. Experimental results obtained in the present study show that the crystallite size of about 7 nm could be obtained by milling elemental Fe and Al powders for 235 hours.
3. A 0.7% change in lattice parameter was observed on mechanical alloying of Fe-47 at. % Al powder for 235 hours.
4. R.M.S. strain kept on increasing during milling and reached to the value of 0.65% after 235 hours of milling.
5. Mechanically alloyed Fe-47 at. % Al powder could be consolidated to the density of 95% of the theoretical at the temperature of 1000°C by applying a pressure of 20 MPa and maintaining it for 20 min. In general, the consolidation behavior of the mechanically alloyed powder was found to vary with temperature and holding time. However, densities higher than 95% of the theoretical value could not be achieved due to the limited capacity of the available hot press.

6. Microstructure of the hot pressed samples was found to contain extremely fine grain structure throughout and contained fine isolated porosity at some locations.

7. It appears that during the ordering treatment at 1000°C for time periods of 9 hrs, 15 hrs and 24 hrs show that the transformation of the structure from predominantly solid-solution state to that of ordered structure begins. Several peaks were found to be present in the X-ray diffraction curves obtained. However, due to the lack of more results and insufficient data in the literature, they could not be clearly discerned.

SUMMARY

In the present investigation iron and aluminium powders, blended in the proportion corresponding to the composition of Fe-47 at% Al, were milled in a high energy attritor mill to synthesize iron and aluminium alloy powders by mechanical alloying technique. Powder samples, taken out at different time intervals from the mill, varying from 15 minutes to 235 hours, were characterized using X-ray diffraction and electron microscopy technique.

Electron microscopy technique was used to illustrate the several stages of mechanical alloying. It was shown that at initial stage particles undergo concurrent deformation, welding and fracturing. The deformation and welding caused formation of flattened flake shaped particles and composite particle containing layers of the alloy component. The cold welding of particles could clearly be seen in the SEM micrographs. Significant variability was observed in the morphology of particles milled for shorter duration of time. However, after long hours of milling, say 40 hrs, it was observed that the particles get more regular and spherical in shape. Composite particles containing alternate layers of iron and aluminium were also observed in the micrographs.

An estimation of the particle sizes, made from the SEM micrographs, revealed that the average particle size increased, in the beginning, from milling time of 15 min to the milling time of 45 min. This illustrated the second stage of mechanical alloying in which the welding of powder particles dominates resulting in increase in the powder particle size. However, it was observed that particle size starts decreasing between the milling time of 45 minutes and 3 hours. This happens because with increasing milling time the hardness of particles increases due to

extensive plastic deformation taking place during mechanical alloying. With further increase in milling time particle size decreased further and after long hours of milling, say 40 hrs, it acquired a steady size. At this stage, there is a reasonable balance between the frequencies of particle fracturing and welding. Therefore the average particle size does not change much during this stage.

X-ray analysis of the powder samples showed that intensities of reflections from elemental Fe and Al decreased with increase in milling time. Strongest aluminium reflection, Al(111), was monitored to study the progress of mechanical alloy. Al(111) reflection became weak with increasing milling time and could not be detected after 40 hours of milling indicating that alloying had completed after 40 hours of milling. No superlattice lines were observed in the X-ray diffraction patterns of the powder samples milled upto 235 hrs. Therefore, it was concluded that no intermetallic compound has formed.

Further analysis of the X-ray diffraction patterns revealed that the peaks got slightly broadened with increase in milling time. However the broadening observed was only small and no substantial broadening or formation of a diffused halo, indicative of the formation of an amorphous phase, was observed. Therefore, it was deduced that no amorphous phase has formed.

The crystallite size and r.m.s. strains were calculated from the observed broadening of the peaks. The crystallite size after 235 hrs of milling was found to 7 nm while the corresponding r.m.s. strain was 0.65%.

Powder particles mechanically alloyed for 235 hours were consolidated using hot pressing technique. Nearly 95% densification was achieved by hot pressing the powders at a temperature of 1000°C for a holding time of 20 min, and at a constant applied pressure of 20 MPa. The

crystallite size of the compact hot pressed at 1000° for 20 min was found to 35 nm which showed that some grain growth has taken place during hot pressing. Several peaks were detected in the X-ray diffraction patterns of the compacts which were given ordering treatment. This suggested the beginning of transformation of the structure from solid-solution state to that of ordered structure.

REFERENCES

1. J.H. Westbrook, Ed., *Mechanical Properties of Intermetallic Compounds*, Wiley, 1959.
2. N.S. Stoloff and R.G. Davies, *Prog. Mater. Sci.*, Vol. 13 (No.1), 1966, p.1.
3. J.H. Westbrook, Ed., *Intermetallic Compounds*, Wiley, 1967.
4. R.W. Guard and J.H. Westbrook, *Trans. AIME*, Vol. 215, 1959, p.807-814.
5. S.M. Copley and B.H. Kear, *Trans. Metall. Soc. AIME*, Vol. 239, 1967, p.977.
6. P.H. Thornton. R.G. Davies, and T. L. Johnston, *Metall. Trans.*, Vol. 1, 1970, p.207.
7. D.P. Pope, *Philos. Mag.*, Vol. 25, 1972, p.917.
8. S. Takeuchi and E. Kuramoto, *Acta Metall.*, Vol. 21, 1973, p.415.
9. V. Paidar, D. P. Pope, and V. Vitek, *Acta Metall.*, Vol. 32, 1984, p. 435.
10. M.H. Yoo, *Sc. Metall.*, Vol. 20, 1986, p.915.
11. M.H. Yoo, J.A. Horton, and C.T. Liu, *Acta Metall.*, Vol. 36, 1988, p.2935.
12. B.H. Kear, C.T. Sims, N.S. Stoloff, and J.H. Westbrook, Ed., *Ordered Alloys - Structural Applications and Physical Metallurgy*, Claitor's Publishing, 1970.
13. C.T. Liu, *Metall. Trans.*, Vol. 4, 1973, p.1743.
14. C.T. Liu and H. Inouye, *Metall. Trans.*, Vol. 10A, 1979, p. 1515.
15. C.T. Liu, *J. Nucl. Mater.*, Vol. 85/86, 1979, p.907.
16. C.T. Liu, *J. Nucl. Mater.*, Vol. 104, 1982, p. 1205.
17. C.T. Liu, *Int. Metall. Rev.*, Vol. 29, 1984, p.168.
18. C.T. Liu, C.L. White, and J.A. Forton, *Acta Metall.*, Vol. 33, 1985, p.213-219.
19. A.I. Taub, S.C. Huang, and K.M. Chang, *Metall. Trans. A*, Vol. 15A, 1984, p.399.

20. *High-Temerature Ordered Intermetallic Alloys*, Materials Research Society Symposia Proceedings, Vol. 39, C.C. Koch, C.T. Liu, and N.S. Stoloff. Ed., Materials Research Society, 1985.

21. *High-Temperature Ordered Intermetallic Alloys II*, Materials Research Society Symposia Proceedings, Vol. 81, N.S. Stoloff, C.C. Koch, C.T. Liu, and O. Izumi, Ed., Materials Research Society, 1987.

22. *High-Temperature Ordered Intermetallic Alloys III*, Materials Research Society Symposia Proceedings, Vol. 133, C.T. Liu, A.I. Taub, N.S. Stoloff, and C.C. Koch, Ed., Materials Research Society, 1989.

23. L.E. Tanner et al., "*Mechanical Behavior of Intermetallic Compounds*," Report AST-TDR62-1087, Manlabs, Inc., 1963-1964, Parts 1-3.

24. H.A. Lipsitt, D. Schechtman, and R.E. Schafrik, *Metall. Trans. A*, Vol. 11A, 1980, p.1369.

25. K. Aoki and O. Izumi, *Acta Metall.*, Vol. 27, 1979, p.807.

26. C.T. Liu, E.H. Lee, and C.G. McKamey, *Scr. Metall.*, Vol. 23, 1989, p.875.

27. C.T. Liu, C.G. McKamey, and E.H. Lee, *Scr. Metall.*, in press.

28. E.A. Aitken, *Intermetallic Compounds*, J.H. Westbrook, Ed., Wiley, 1967, p.491-516.

29. A.J. Bradley and A. Taylor, *Proc. R. Soc. (London) A*, Vol. 136, 1932, p.210.

30. A.J. Bradley and A. Taylor, *Proc. R. Soc. (London) A*, Vol. 159, 1937, p.56.

31. N. Ridley, *J. Inst. Metl*, Vol. 94, 1966, p.255.

32. M.J. Cooper, *Philos. Mag.*, Vol. 8, 1963, p.805.

33. S. Ohiai, Y. Oya, and T. Suzuki, *Acta Metall.*, Vol. 32, 1984, p.289-298.

34. R.L. Fleischer, *Acta. Metall.*, Vol. 11, 1963, p.203.

35. C.T. Liu, C.L. White and E.H. Lee, *Scr. Metall.*, Vol. 19, 1985, p.1247-1250.

36. B.H. Rabin and R. N. Wright, *Met. Trans. A*, Vol. 22A, 1991, p.277.

37. C.T. Ho, C.J. Cheng, and J. A. Sekhar, *Metall. Trans. A*, Vol. 22A, 1991, p.225.

38. I. Baker and D.J. Gaydosh, *Mater. Sci. Eng.*, Vol. 96, 1987, p.147.

39. D.J. Gaydosh, S.L. Draper, and M.V. Nathal, *Metall. Trans. A*, Vol. 20A, 1984, p.304-321.

40. C.G. McKamey, J.A. Horton, and C.T. Liu, in *High- Temperature Ordered Intermetallic Alloys II*, Materials Reseach Society Symposia Proceedings, Vol. 81, N.S. Stoloff, C.C. Koch, C.T. Liu, and O. Izumi, Ed., Materials Research Society, 1987, p. 321-327.

41. W.R. Kerr, *Metall. Trans. A*, Vol. 17A, 1986, p.2298.

42. M.G. Mendiratta, S. K. Ehlers, and D.K. Chatterjee, in *Rapid Solidification Processing : Principles and Technologies*, National Bureau of Standards, 1983, p. 420.

43. P. Morgnand, P. Mouturat, and G. Sainfort, *Acta Metall.*, Vol. 16, 1968, p.807.

44. S. Strothers and K. Vendula, in *Proceedings of the Powder Metallurgy Conference*, Vol. 43, Metal Powder Industries Federation, 1987, p.597.

45. M. G. Mendiratta. H. K. Kim, and H. A. Lipsitt, *Metall. Trans. A*, Vol 15A, 184, p. 395.

46. Y. Umakoshi and M. Yamaguchi, *Philos. Mag. A*, Vol. 44, 1981, p. 711.

47. T. Takasugi and O. Izumi, *Acta Metall.*, Vol. 34, 1986, p. 607.

48. N. Masahashi, T. Takasugi, and O. Izumi, *Metall Trans. A*, Vol. 19A, 1988, p. 353.

49. O. Izumi and T. Takasugi, *J. Mater. Res.*, Vo. 3, 1988. p. 426.

50. T. Takasugi, N. Masahashi, and O. Izumi, *Scr. Metall.*, Vol. 20, 1986, p. 1317.

51. N. Masahashi. T. Takasugi, and O. Izumi, *Acta Metall.*, Vol. 36, 1988, p. 1923-1836.

52. T. Takasugi, and O. Izumi, *Scr. Metall.*, Vol. 19, 1985, p. 903-907.

53. A. K. Kuruvilla, S. Ashok, and N. S. Stoloff, in *Proceedings of the Thrid International Congress on Hydrogen in Metals*, Vol. 2, Pergamon Press, 1982, p. 629.

54. A. K. Kuruvilla and N. S. Stoloff, and D. J. Duquette, *Acta Metall.*, Vol. 19, 1985, p. 83.

55. G. M. Camus, N. S. Stoloff, and D. J. Duquette, *Acta Metall.*, Vol. 37, 1989, p. 1497-1501.

56. M. A. Crimp and K. Vedula, *J. Mater. Sci.*, Vol. 78, 1986, p. 193.

57. K. Vedula and J. R. Stephens, in *High-Temperataure Ordered Intermetallic Alloys II*, Materials Research Society Symposia Proceedings, Vol. 81, N. S. Stoloff, C. C. Koch, C.T. Liu, and O. Izumi, Ed., Materials Research Society, 1987, p. 381-391.

58. I. Jung, M. Rudy, and G. Sauthoff, in *High-Temperature Ordered Intermedallic Alloys II*, Materials Research Society Symposia Proceedings, Vol. 81, N. S. Stoloff, C. C. Koch, C.T. Liu, and O. Izumi, Ed., Materials Research Society, 1987, p. 263-274.

59. S. A. David et al., *Weld. J.*, Vol. 68, 1989, p. 372s-381s.

60. B. Schmidt, P. Nagpal, and I. Baker, in *High-Temperature Ordered Intermetallic Alloys III*, Mateials Research Society Symposia Proceedings, Vol. 133, C.T. Liu, A.I. Taub, N.S. Stoloff, and C.C. Koch, Ed., Materials Research Society, 1989, p. 755-760.

61. J.H. DeVan, in *Oxidation of High-Temperature Intermetallics*, T. Grobstain and J. Doythak, Ed., TMS, 1989.

62. C.G. McKamey, J.A. Horton and C.T.Liu, *High-Temperature Ordered Intermetallic Alloys II*, ed., by N. S. Stoloff, C.C. Koch, C.T. Liu and O. Izumi, MRS Symp. Proc., Vol. 81, MRS, Pittsburgh, (1987), p. 321.

63. M.G. Mendiratta, S. K. Ehlens and H. A. Lipsitt, *Metall. Trans. A*, 18A, 1987, p. 509.

64. A. K. Mishra, *Metall. Trans. A.*, 21A, 1990, p. 441.

65. S. L. Draper, D. J. Gaydosh, M. V. Nathal and A. K. Mishra, *J. Mater, Res.*, 5, 1990, p. 1976.

66. J. A. Moser, M. Aindow, W.A.T. Clark, S. Draper and H. I. Fraser, *Intermetallic Matrix Composites*, ed., by D. L. Adam, P. L. Martin, D. V. Miracle and R. B. McMeeking, MRS Symp. Prod., Vol. 194, MRS, Pittsburgh, 1990, p. 379.

67. K. M. Vedula, *Mater. Manuf. Process.*, Vol. 4, 1989, p. 57.

68. S. D. Strothers and K. Vedula, *Prog. Powder Metallurgy*, 1087, 597.

69. K. Vedula and J. R. Stephens, *Prog. Powder Metallurgy*, (1987), 561.

70. Benjamin, J. S., *Met. Trans.*, Vol. 1, 1970, 1-9.

71 D. R. Maurice and T. H. Courtney, *Met. Trans.*, Vol. 21A, 1990, p. 289-303.

72. B.J.M. Aikin and T.H. Courtney, *Met. Trans.*, Vol. 24A, 1993, p. 647-657.

73. C. C. Koch, *Nanostr. Mater.*, Vol.2, 1993, p.109.

74. T.R. Anantharaman and C. Suryanarayana, *Rapidly solidified metals: A technological overview* (Aedermannsdorf, Switzerland: Trans Tech Publ.), 1987.

75. H. H. Liebermann (Ed.), *Rapidly Solidified alloys: Processes, Structures, Properties and Applications*, (New York: Marcel Dekker, Inc.), 1993.

76. N. El-Kaddah (Ed.), *Thermal plasma applications in materials and metallurgical processing* (Warrendale, PA: TMS), 1992.

77. R. Birringer, *Mater. Sci. Engg.*, Vol. A117, 1989, p.33.

78. D. Turnbull, *Met. Trans.*, Vol. A12, 1981, p.695.

79. R. Birringer, H. Gleiter, H. P. Klein and P. Marquart, *Phys. Lett.*, Vol. A102, 1984, p.365.

80. B.H. Kear and L.E. McCandlish, *Nanostr. Mater.*, Vol. 3, 1993, p.19.

81. H. Chang, C.J. Altstter and R. S. Averback, *J. Mater. Res.*, Vol. 7, 1992, p.2962.

82. D.S. Lashmore and M.P. Dariel, in *Encyclopedia of Materials Science and Engineering*, (Ed). R.W. Cahn (Oxford, UK: Pergamon) suppl. Vol. 1, 1988, p.136-140.

83. J. J. Ritter, D.B. Minor, R.D. McMichael and R.D. Shull, in *Nanophases and nancrystalline structures*, (eds.) R.D. Shull and J. M. Sanchez (Warrendale, PA: TMS), 1993, p.33-40.

84. Roy, R.A., Roy, R., *Mater. Res. Bull.*, Vol. 19, 1984, p. 169.

85. D. A. Rigney, *Ann. Rev. Matter. Sci.*, Vol 18, 1988, p.141.

86. A.E. Berkowitz and J. L. Walter, *J. Mater. Res.*, Vol. 2, 1987, p.277.

87. C.H. Chou and J. Phillips, *J. Mater. Res.*, Vol. 7, 1992, p.2107.

88. M. L. Mandich, V.E. Bondybey and W.D. Reents, *J. Chem. Phys.*, Vol. 86, 1987, p.4245.

89. G.W. Kriechbaum and P. Kleinschmitt, *Adv. Mater.*, Vol. 1, 1989, p.330.

90. V. Haas, H. Gleiter and R. Birringer, *Scr. Metall, Mater.*, Vol. 24, 1990, p. 1529.

91. J. S. Benjamin, *Sci. Am.*, Vol. 234, 1976, p.40.

92. Hellstern, Fecht, H.J., Fu, Z., Johnson, W.L., *J. Appl. Phys.*, Vol. 65, 1989a, p. 305.

93. Fu, Z., Fecht, H.J., Johnson, W.L., *MRS Symposium Proceedings*, Vol. 186, 1990.

94. Gaffet, E., Harmelin, M., *J. Less Common Metals*, Vol. 157, 1990, p. 210.

95. Hellstern, E., Fecht, H.J. Garland, C., Johnson, W.L., *Mater. Res. Soc. Symp. Proc.*, Vol. 132, 1989b, p. 139.

96. Jang, J.S.C., Koch, C.C., *J. Mater. Res.*, Vol. 5, 1990b, p. 498.

97. Schlump, W., Grewe, H., in New Materials by Mechanical Alloying Techniques : Aizt, E., Schult, L. (Eds.), Oberursel : DGM Informations Gesellschaft., 1989, p. 307.

98. Shingu, P.H., Huang, B., Nishitani, S.R., Nasu, S., *Suppl. to Trans. JIM*, 1988, Vol. 29, p. 3.

99. Koch, C.C., *Annu. Rev. Mater. Sci.*, Vol. 19, 1989, p. 121.

100. Shingu, P.H., Huang, B., Kuyama, J., Ishihara, K. N., Nasu, S., in New Materials by Mechanical Alloying Techniques : Aizt, E., Schultz, L. (Eds.), Oberursel : DGM. Informations gessllschaft, 1989, p. 319.

101. Ermakov, A.E., Yurchikov, E.E., Barinov, V.A., *Phys. Met. Metall.*, Vol. 54, 1981, p. 50.

102. Ermakov, A.E., Barinov, V.A., Yurchikov, E.E., *Fiz. Metal Melalloved*, Vol. 54, 1982, p. 50.

103. Weeber, A.W., Bakker, H., *Physica B*, Vol. 153, 1988, p. 93.

104. White, R.L., Nix, W.D., in New Developments and Applications in Composites : Khulmann Wilsdorf, D., Harugan, W.C. (Eds.), Warrendale (PA): TMS, 1979, p. 78.

105. Koch, C.C., Cavin, O.B., McKamey, C.G., Scarbrough, J.O., *Appl. Phys. Lett.*, Vol. 43, 1983, p. 1017.

106. Wang, G., Zhang, D. Chen, H., Liu B, Wang, W., Dong, Y., *Phys. Lett. A*, Vol. 155, 1991, p. 57.

107. Schwarz, R.B., Petrich, R.R., Saw, C.K., *J. Non-Cryst. Solid*, Vol. 76, 1985, p. 281.

108. Hellstern, L.E., Schultz, L., *Appl. Phys. Lett.*, Vol. 48, 1986, p. 124.

109. Schwarz, R.B., Koch, C.C., *Appl. Phys. Lett.*, Vol. 49, 1986, p. 146.

110. Schwarz, R.B., Johnson, W.L., *Phys. Rev. Letts*, Vol. 51, 1983, p. 415.

111. Schwart, R.B., Pefnich, R.R., *J. Less - Common Metals*, Vol. 140, 1988, p. 171.

112. Rolgin, B.P., Vanek, M.A., McKory, T., Ham, D.J., *J. Non-Cryst. Solids*, Vol. 87, 1986, p. 281.

113. Hellstern, E., Schlutz, L., Bormann, R., Lewe, D, *Appl. Phys. Lett.*, Vol. 53, 1988, p. 1399.

114. Koch, C.C., Kim, M.S., *J. Physique*, Vol. 46, 1985, p. C8-573.

115. Kim, M.S., Koch, C.C., *J. Appl. Phys.*, Vol. 62, 1987, p. 3450.

116. Lee, P.Y., Jang, J., Koch, C.C., *J. Less Common Metals*, Vol. 140, 1988, p. 73.

117. Veltl, G., Schloz, B., Kunze, H.D., *Mater. Sci. Engg.*, 1991, A134987.

118. El-Eskandarany, M.S., Itoh, F., Aoki, K., Suzuki, R., *J. Non-Cryst. Solids*, 1990, 117/118, 729.

119. Schlutz, L., 1988, *Mater. Sci. Engg.*, Vol. 97, 1988, p. 15.

120. Cocco, G., Soklltta, I, Batterztati, L., Baricco, M., Ehzo, S., *Philos Mag.*, Vol. B61, 1980, p. 473.

121. Bonetti, E., Cocco, G., Ehzo, S., Valde, G., *Mater. Sci. Tech.*, Vol. 6, 1990, p. 1258.

122. Murty, B.S., *Bull. Mater. Sci.*, Vol. 16, Feb. 1993, No. 1, p. 1-17.

123. Matsuki, K., Inove, A., Kimura, H.M., Masumoto, T., 1988, *Mater. Sci. Engg.*, Vol. 97, 1988, p. 47.

124. Sundaresan, R., Jackson, A.G., Mrishna Murthy, S., Froes, F.H., *Mater. Sci. Engg.*, Vol. 97, 1988, p. 115.

125. Murty, B.S., Mohan Rao, M., Ranganathan, S., *Scr. Metall.*, Vol. 24, 1990, 1819.

126. Koch, C.C., *Nanostr. Mater.*, Vol. 2, 1993, p. 109-129.

127. Koch, C.C., in Processing of Metals and Alloys, Vol. 15, Materials Science and Technology - A Comprehensive Treetment, ed. R.W. Cahn, (Weinheim Germany: VCH, 1991), p. 193-245.

128. Suryanaryana, C., Froes, F.H., *Mater Sci. Forum*, Vol. 88-90, 1992, p. 445-452.

129. deBabadello, J.J., Froes, F.H., Schwarz, R. (Eds.), Structural Applications of Mechanical Alloying, Materials Park, OH, ASM, 1993.

130. Suryanarayana, C., Froes, F.H., Mukopadhyay, D.K., Gizmich, G., Chen, G.H., Peng, Z., Mishurda, J. in Processing and Fabrication of Advanced Materials III, Ravi, V.A., Srinvan, T.S., Moore, J.J., (Eds.), The Minerals, Metals and Materials Society, 1994.

131. Fair, G.H., Wood, J.V., *Powder Metallurgy*, Vol. 36, 1993, No. 2.

132. Olezak, D., Shungu, P.H., *Materials Science and Engineering*, Vol. A181/A182, 1994, p. 1217-1221.

133. Polkin, I.S., Kaputkin, E., Ja Boizov, A.B., ASM International Conference of Structural Applications of Mechanical Alloying, Myrtle Beach (SC), March 27-29, 1990, p. 25.

134. Lee, P.Y., Koch, C.C., *J. Non-Crystl. Solids*, Vol. 94, 1987, p. 88.

135. Oehring, M., Bormann, R., *J. Phys. France (Collogues)*, Vol. 51, 1990, 164-169.

136. Ivanov, E., Gryorieva, T., Gdulokova, G., Boldylev, V., Fasman, A.B., Mikhailenko, S.D., Kalining, O.T., *Mater. Lett.*, Vol. 7, 1988, p. 57.

137. Frattini, R., Schiffini, L., Scipone, G., Bonetti, E., Enzo, S. in Processing, Properties and Applications of Iron Aluminides: Schneibel, J.H, Crimp, M.A. (Eds.), The Minerals, Metals & Materials Society, 1994, p. 79-88.

138. Sundaresan, R., Froes, F.H., in New Materials by Mechanical Alloying Techniques : Arzt, E., Schultz, L. (Eds.), Oberusel : DGM Informations gesellschaft, 1989, p. 253.

139. Gaffet, E., Gaspaid, J.P., *J. Phys. France (Colloques)*, Vol. 57, 1990, C4-205.